AD-760 573

The Relationship of Structure to Properties in Graphite Fibers

Rensselaer Polytechnic Institute

prepared for

Air Force Materials Laboratory

OCTOBER 1971

Distributed By:

NTIS

National Technical Information Service
U. S. DEPARTMENT OF COMMERCE

RELATIONSHIPS OF STRUCTURE TO PROPERTIES IN CARBON FIBERS, PART I

Russell J. Diefendorf

Edward W. Pokarsky

Technical Report AFML-TR-72-133, Part I

October 1971

Air Force Materials Laboratory
Air Force Systems Command
Wright-Patterson Air Force Base, Ohio

NOTICE

When Government drawings, specifications, or other data are used for any purpose other than in connection with a definitely related Government procurement operation, the United States Government thereby incurs no responsibility nor any obligation whatsoever; and the fact that the government may have formulated, furnished, or in any way supplied the said drawings, specifications, or other data, is not to be regarded by implication or otherwise as in any manner licensing the holder or any other person or corporation, or conveying any rights or permission to manufacture, use, or sell any patented invention that may in any way be related thereto.

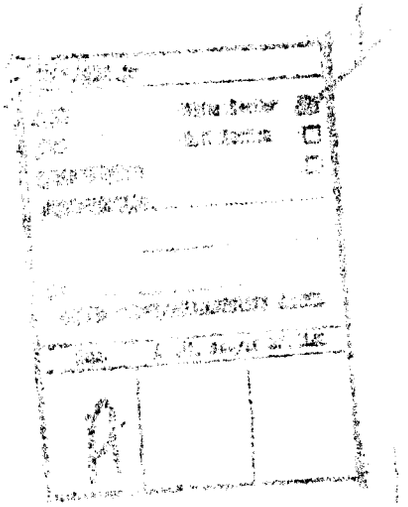

Return of this report should not be returned unless return is required by security requirements, contractual obligations, or notice on a specific document.

Unclassified

Security Classification

DOCUMENT CONTROL DATA - R&D

(Security classification of title, body of abstract and indexing annotation must be entered when the overall report is classified)

1. ORIGINATING ACTIVITY (Corporate author)	2a. REPORT SECURITY CLASSIFICATION
Rensselaer Polytechnic Institute Materials Division, Troy, New York 12181	Unclassified
	2b GROUP

3. REPORT TITLE

THE RELATIONSHIP OF STRUCTURE TO PROPERTIES IN GRAPHITE FIBERS

4. DESCRIPTIVE NOTES *(Type of report and inclusive dates)*

5. AUTHOR(S) *(Last name, first name, initial)*

Diefendorf, Russell J.
Tokarsky, Edward W.

6. REPORT DATE	7a. TOTAL NO. OF PAGES	7b. NO. OF REFS
	84 96	5

8a. CONTRACT OR GRANT NO.	9a. ORIGINATOR'S REPORT NUMBER(S)
b. PROJECT NO.	AFML-TR-72-133
c.	9b. OTHER REPORT NO(S) *(Any other numbers that may be assigned this report)*
d.	

10. AVAILABILITY/LIMITATION NOTICES

11. SUPPLEMENTARY NOTES	12. SPONSORING MILITARY ACTIVITY
	Air Force Materials Laboratory Wright-Patterson AFB, Ohio

13. ABSTRACT

Three-dimensional structural models of a range of carbon fibers having several precursor bases and widely differing moduli and strengths have been developed. Experimental techniques employed included x-ray and electron diffraction; and electron, scanning electron, and optical polarized light microscopies; additionally, a new etching technique, reverse radio frequency sputtering was shown to reveal fiber internal structural features.

Results show that the morphology of the basic structural unit of carbon fibers is that of rippled ribbons consisting of parallel layers of basal planes. With increasing moduli the ribbons become progressively thicker, straighter and better aligned with respect to the fiber axis. An associated development of a radial preferred alignment occurs with increasing modulus. In some very high modulus fibers, preferred orientation of the crystallographic a-axis exists.

The combination of radial and axial structural information is used to explain some aspects of fiber mechanical behavior. A better aligned axial structure gives a higher tensile modulus, but the bonding between adjacent ribbons in the fiber decreases altering the fiber fracture mode and strength. Along with the overall increasing axial alignment with modulus, the fiber surface progressively develops a more basal plane character; this is the chief cause of shear strength problems in higher modulus carbon fiber composites.

(over)

DD FORM 1 JAN 14 1473

Security Classification

14. KEY WORDS	LINK A		LINK B		LINK C	
	ROLE	WT	ROLE	WT	ROLE	WT
Carbon and graphite fibers, structure-property relations, 3-dimensional structural models, x-ray and electron diffraction, electron and scanning electron microscopy, polarized light microscopy, reverse RF sputter etching						

Gradients in axial preferred orientation not only give rise to non-uniform loading of the fiber from surface to core, but also to residual stresses on cooling from final heat treatment temperature which lower the fiber surface flaw sensitivity; the radial texturing is responsible for residual stresses which generate interior flaws.

In summary, these results show that carbon fibers should not be treated in composite mechanical analyses as structurally monolithic reinforcements.

INSTRUCTIONS

1. ORIGINATING ACTIVITY: Enter the name and address of the contractor, subcontractor, grantee, Department of Defense activity or other organization *(corporate author)* issuing the report.

2a. REPORT SECURITY CLASSIFICATION: Enter the overall security classification of the report. Indicate whether "Restricted Data" is included. Marking is to be in accordance with appropriate security regulations.

2b. GROUP: Automatic downgrading is specified in DoD Directive 5200.10 and Armed Forces Industrial Manual. Enter the group number. Also, when applicable, show that optional markings have been used for Group 3 and Group 4 as authorized.

3. REPORT TITLE: Enter the complete report title in all capital letters. Titles in all cases should be unclassified. If a meaningful title cannot be selected without classification, show title classification in all capitals in parenthesis immediately following the title.

4. DESCRIPTIVE NOTES: If appropriate, enter the type of report, e.g., interim, progress, summary, annual, or final. Give the inclusive dates when a specific reporting period is covered.

5. AUTHOR(S): Enter the name(s) of author(s) as shown on or in the report. Enter last name, first name, middle initial. If military, show rank and branch of service. The name of the principal author is an absolute minimum requirement.

6. REPORT DATE: Enter the date of the report as day, month, year, or month, year. If more than one date appears on the report, use date of publication.

7a. TOTAL NUMBER OF PAGES: The total page count should follow normal pagination procedures, i.e., enter the number of pages containing information.

7b. NUMBER OF REFERENCES: Enter the total number of references cited in the report.

8a. CONTRACT OR GRANT NUMBER: If appropriate, enter the applicable number of the contract or grant under which the report was written.

8b, 8c, & 8d. PROJECT NUMBER: Enter the appropriate military department identification, such as project number, subproject number, system numbers, task number, etc.

9a. ORIGINATOR'S REPORT NUMBER(S): Enter the official report number by which the document will be identified and controlled by the originating activity. This number must be unique to this report.

9b. OTHER REPORT NUMBER(S): If the report has been assigned any other report numbers *(either by the originator or by the sponsor)*, also enter this number(s).

10. AVAILABILITY/LIMITATION NOTICES: Enter any limitations on further dissemination of the report, other than those imposed by security classification, using standard statements such as:

(1) "Qualified requesters may obtain copies of this report from DDC."

(2) "Foreign announcement and dissemination of this report by DDC is not authorized."

(3) "U. S. Government agencies may obtain copies of this report directly from DDC. Other qualified DDC users shall request through _____."

(4) "U. S. military agencies may obtain copies of this report directly from DDC. Other qualified users shall request through _____."

(5) "All distribution of this report is controlled. Qualified DDC users shall request through _____."

If the report has been furnished to the Office of Technical Services, Department of Commerce, for sale to the public, indicate this fact and enter the price, if known.

11. SUPPLEMENTARY NOTES: Use for additional explanatory notes.

12. SPONSORING MILITARY ACTIVITY: Enter the name of the departmental project office or laboratory sponsoring *(paying for)* the research and development. Include address.

13. ABSTRACT: Enter an abstract giving a brief and factual summary of the document indicative of the report, even though it may also appear elsewhere in the body of the technical report. If additional space is required, a continuation sheet shall be attached.

It is highly desirable that the abstract of classified reports be unclassified. Each paragraph of the abstract shall end with an indication of the military security classification of the information in the paragraph, represented as *(TS), (S), (C), or (U)*.

There is no limitation on the length of the abstract. However, the suggested length is from 150 to 225 words.

14. KEY WORDS: Key words are technically meaningful terms or short phrases that characterize a report and may be used as index entries for cataloging the report. Key words must be selected so that no security classification is required. Identifiers, such as equipment model designation, trade name, military project code name, geographic location, may be used as key words but will be followed by an indication of technical context. The assignment of links, rules, and weights is optional.

AFML-TR-72-133

Part I

THE RELATIONSHIPS OF STRUCTURE TO PROPERTIES IN GRAPHITE FIBERS, PART I

Russell J. Diefendorf

Edward W. Tokarsky

FOREWORD

This report was prepared by R. J. Diefendorf and E. W. Tokarsky, Materials Division, Rensselaer Polytechnic Institute under Contract AF33(615)-70-C-1530 entitled "The Relationship of Structure to Properties in Graphite Fibers". It was administered by the Air Force Materials Laboratory, Air Force Systems Command, Wright-Patterson Air Force Base, Herbert M. Ezekiel (AFML/MBC), project monitor.

Gratefully acknowledged is the scanning electron microscope work of Mr. John Nelson of Rensselaer Polytechnic Institute. Particular thanks is due to Dr. Christopher LeMaistre for many ideas originating from discussions of the effects of structure on mechanical behavior of carbon fibers. Schematic diagrams on pages 2, 3 and 4 were reproduced from the Ph.D. thesis of Dr. Barry Butler, R.P.I., 1969. Also, special thanks is due to Mr. Herbert Ezekiel of the Air Force, who supplied a number of experimental high performance fibers.

This report covers research conducted during the period May 1970 to April 1971.

This report was submitted by the authors in October 1971.

This technical report has been reviewed and is approved.

T. J. Reinhart Jr.

T. J. REINHART, JR., Actg. Chief
Composite & Fibrous Materials Branch
Nonmetallic Materials Division

Abstract

Three-dimensional structural models of a range of carbon fibers having several precursor bases and widely differing moduli and strengths have been developed. Experimental techniques employed included x-ray and electron diffraction; and electron, scanning electron, and optical polarized light microscopies; additionally, a new etching technique, reverse radio frequency sputtering was shown to reveal fiber internal structural features.

Results show that the morphology of the basic structural unit of carbon fibers is that of rippled ribbons consisting of parallel layers of basal planes. With increasing moduli the ribbons become progressively thicker, straighter and better aligned with respect to the fiber axis. An associated development of a radial preferred alignment occurs with increasing modulus. In some very high modulus fibers, preferred orientation of the crystallographic a-axis exists.

The combination of radial and axial structural information is used to explain some aspects of fiber mechanical behavior. A better aligned axial structure gives a higher tensile modulus, but the bonding between adjacent ribbons in the fiber decreases altering the fiber fracture mode and strength. Along with the overall increasing axial alignment with modulus, the fiber surface progressively develops a more basal plane character; this is the chief

cause of shear strength problems in higher modulus carbon fiber composites.

Gradients in axial preferred orientation not only give rise to non-uniform loading of the fiber from surface to core, but also to residual stresses on cooling from final heat treatment temperature which lower the fiber surface flaw sensitivity; the radial texturing is responsible for residual stresses which generate interior flaws.

In summary, these results show that carbon fibers should not be treated in composite mechanical analyses as structurally monolithic reinforcements.

TABLE OF CONTENTS

TABLES

SECTION I

INTRODUCTION

Graphite has a hexagonal close packed crystal structure which in the two directions of the basal plane is strong and stiff, and in the third direction, perpendicular to the basal plane, is weak and compliant. High performance carbon fibers must make use of the strong directions without suffering from the poor properties of the third. Obviously, the graphite layer planes must be aligned parallel to the fiber axis if high modulus and high strength are to be achieved, but high alignment will accentuate the poor shear and tensile strength between the planes. A strong fiber microstructure would most likely consist of small elongated grains. Much invaluable research has shown that carbon fibers basically consist of small wrinkled ribbons aligned approximately parallel to the fiber axis. Most of this work has centered on the axial microstructure, particularly at the ultrastructure level, where the individual basal planes in the wrinkled ribbons can be resolved. While the wrinkled ribbon model gives an approximate estimate for fiber modulus, it provides little information of what the strength of a fiber will be or how the fiber will perform in a composite.

Shown schematically below is an idealized simple composite member consisting of a single high modulus fiber in a more compliant matrix; the parallel vertical lines can be thought of

as strain markers embedded in the sample.

AS CAST

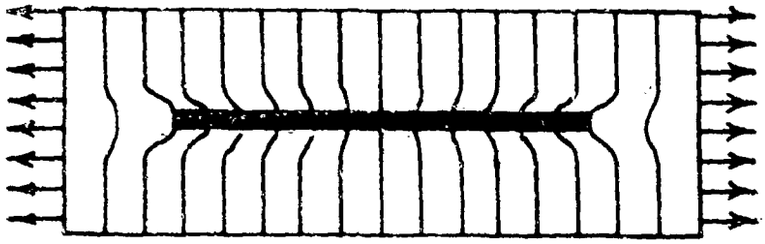

STRESSED

If the member is now stressed in uniaxial tension both the filament and matrix dilate, but because of the mismatch in modulus concentric shear stress gradients are generated in the matrix and fiber. Over-simplifying the situation for the sake of illustration, three initial modes of composite failure are possible: failure of the matrix in tension, fracture of the filament in tension, or fiber-matrix interfacial debonding via shear failure. The last mode is one of great concern in graphite fiber composite systems;firstly, the maximum shear stress that the interface can withstand for higher modulus carbon fibers is low: secondly, the interfacial bond

strength determines the sensitivity of a composite to flaws. A measure of the tendency to fail in interfacial shear is given in the short beam shear strength test illustrated below.

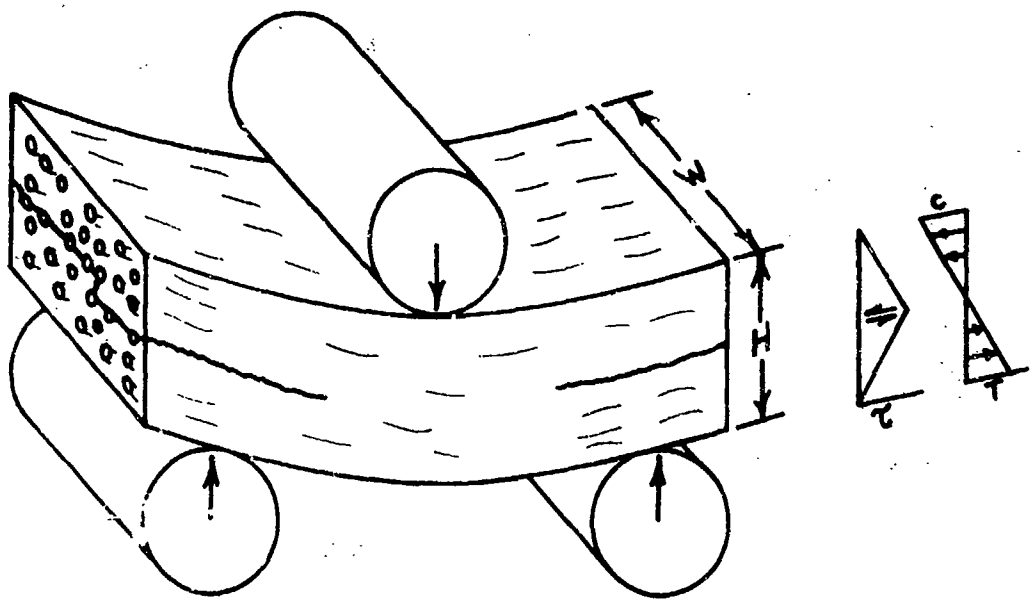

Here a short segment of a composite sample is stressed as shown in a three-point bending configuration. The relative state of stress is indicated to the right of the sample. As illustrated, what is often found is initial failure in the region of maximum shear stress and not in tension or compression. The dependence of this effect on fiber modulus is given in the following plot. Surface treatment increases shear strength but the decrease in shear strength with increasing fiber modulus still remains.

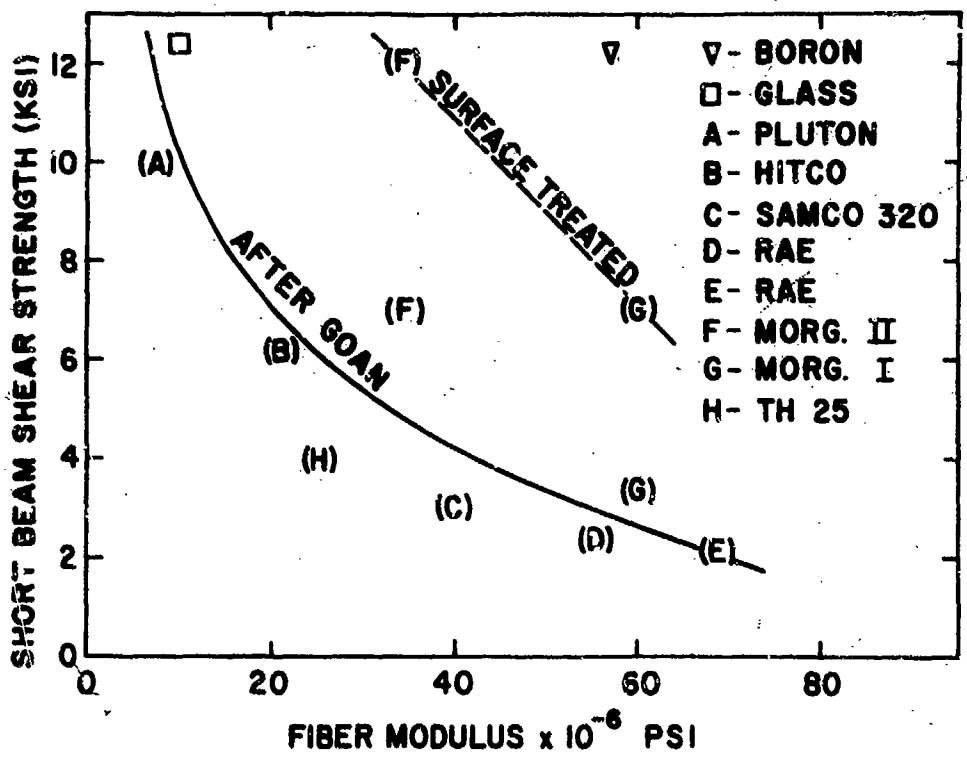

The short beam shear strength of a composite containing 58 msi boron fibers is about 14,000 psi, whereas an untreated carbon fiber sample of similar modulus would fail at 2,000 psi. From a practical standpoint it is important to know if the interface problems are related to fabrication methods, or are inherent to the materials involved, or both. The degree to which the matrix wets and bonds to the reinforcement is of concern. Earlier studies show that if the surfaces of the constituent fibers are of high basal character, wetting can be a severe problem. However, a high degree of basal edge exposure on the fiber surface would

promote a greater volume fraction of bonded interface as well as larger specific interfacial shear strengths. This strong interfacial bond may give too brittle a composite for the particular fiber and resin used. A knowledge of fiber surface structures is of great importance in understanding interfacial bonding.

The load imposed on a composite member is transferred to each fiber via a shear stress. As the evidence provided later in this report suggests, each fiber must not be thought of as a homogeneous anisotropic entity, but rather as a more or less cyclindrically symmetric collection of anisotropic units linked such that the fiber may be viewed as a composite system in its own right. As such, the moduli of the individual fibers will depend on the details of the axial preferred orientation in each fiber structure, while the strength will be a function not only of surface flaws and related effects, but of the axial as well as radial textures and gradients present. The strength of a given fiber will depend on how efficiently the shear stress at and near the interface can be uniformly transferred to the fiber core. Also, potentially significant amounts of residual stress may be present in each fiber; the importance of this inference cannot be dismissed since the proper control of such a factor in a brittle material can have a major impact on strengths, or strain to failure.

These interpretations infer that the structure of many types of carbon fibers must be known essentially in three dimensions from

the scale of the fiber diameter to at least the ultrastructural level. The contribution of the present work stems, in part, from the more general approach taken in which a number of commercial and experimental carbon fibers having different precursor bases and a very wide range of mechanical properties have been structually modeled in three dimensions in order to clarify some of the practical consequences of structure. Additionally, some insight has been gained in various aspects of processing conditions which ultimately affect the fiber and thus composite performance.

SECTION II

TECHNIQUES

Past research on carbon fibers has emphasized the axial structure. While this is an indispensable part of fiber characterization, the work at R.P.I. has shown this to be insufficient for a complete description of carbon fiber behavior[1]. In particular, little work has been done on radial structural distributions and the consequences of this structure on fiber performance. Furthermore, past research has determined the structure of carbon fibers at the atomic level (≈ 3 Å resolutions) or the fibrillar level (≈ 100 Å resolutions) but has neglected the gross structural variations at the fiber diameter level. Since the purpose of this study was to determine the three dimensional structures of a variety of carbon fibers ranging from low to high modulus, several new techniques were added to those previously used to describe axial structure.

The major technological problem in making carbon fibers is how to attain a high alignment of these basal planes parallel to the fiber axis, while preserving some shear strength within the fiber and at the fiber surface. In this sense, much of the literature is concerned with accurate descriptions of preferred orientations of the basal plane. Of course, within any one sample a distribution of structural perfection may exist and this variation must also be determined.

In the case of high modulus carbon fibers the most striking feature is the high preferred orientation of the basal planes that can be obtained with respect to the fiber axis. Although the formation of this well aligned final structure from the precursor is not as yet fully understood, many of the important details can be resolved with the following techniques:

1) X-ray Diffraction
2) Electron Diffraction
3) Bright field, Dark field, and Replication Electron Microscopy
4) Scanning Electron Microscopy (SEM)
5) Optical Polarized Light Microscopy
6) Reverse R.F. Sputtering of Fibers.

1. X-Ray Diffraction

For a carbon fiber 10μ or less in diameter, x-ray diffraction information reflects the character of the total volume of the fiber.

Debye-Scherrer photographs of bundles of collimated fibers enabled qualitative assessments to be made of preferred orientations, crystallite sizes, three dimensional ordering, and small angle scattering. For quantitative measurements of atomic spacings, crystallite size, and preferred orientation, diffractometry was used. Instrumental broadening of the diffractometer traces were determined by running a very well annealed sample (3600°C for 16 hours) of pyrolytic graphite. In cases where small crystallite sizes were present, corrections to the raw data were made using essentially the procedure of Heckman[2]. A description of this correctional scheme is given in Appendix I.

2. Electron Diffraction

Whereas the x-ray results give average fiber characteristics, the penetration of an electron beam is only hundreds of angstroms, thus giving information about fiber surface structures. Using a Hitachi Model HS-7 electron microscope employing an accelerating potential of 50 kV, electron diffraction patterns were obtained for the fibers studied and qualitatively assessed. Subsequent comparison of x-ray and electron diffraction revealed any gross differences between surface and average fiber structures.

3. Electron Microscopy

Carbon extraction replicas of fiber sides and ends were prepared using chromium as shadowing material. These replicas provided high resolution of surface textures, particularly along the fiber sides.

The bright field technique was used to study the profiles of fibers fractured in bending.

Dark field technique was stressed in this study, particularly the (0002) dark field, since it provides information about basal preferred orientation; in selected cases the $(10\bar{1}0)$ dark field was also used. In addition, crystallite sizes could be directly measured.

4. Scanning Electron Microscopy (SEM)

SEM provides magnifications intermediate between optical and electron microscopy. Textures of sides and fractured ends of fibers could be observed as well as overall composite fracture characteristics.

5. Polarized Light Analysis

The interaction of vertically incident plane polarized light with polished cross sections of carbon fibers may be used to determine radial basal distributions. Using the optical theory given in Appendix II, it has been possible to semi-quantitatively radially characterize several fibers used in this study.

6. Reverse Radio Frequency Sputtering

The ability to progressively and controllably etch away without damage the outer surface of a carbon fiber is desirable. Such an etch would remove any smeared graphitic material for optical measurements and facilitate further development of structural characterization using electron diffraction. A non-damaging thinning appears possible with radio-frequency (R.F.) reverse sputtering, a process in which inert gas ions bombard a target material, in this case

fibers mounted in an epoxy matrix, under the influence of a controlled power R.F. field.

FIBERS

Table I lists the fibers studied in this project. Fibers with the CS code designation along with their corresponding mechanical properties were supplied by the U.S. Air Force through Mr. Herbert Ezekiel. The modulus and strength ranges are extensive allowing a potentially large spectrum of structures to be studied. WYB is a commercial graphite fiber of Union Carbide Corp. manufactured from Villwyte rayon yarn. CS-2 fiber was prepared from an experimental polyacrylonitrile (PAN) homopolymer wet spun yarn, and was surface treated. Fortafil 5-Y is a surface treated commercial graphite fiber (Great Lakes Carbon Corp.) prepared from PAN yarn. CS-4 is an experimental graphite fiber prepared from a commercial carbon yarn, VYB 70-½ (Union Carbide Corp.) by a catalytic graphitization process (British provisional specification 1,295,289, H. M. Ezekiel); the yarn was not surface treated. CS-1 fiber was made from an experimental high tenacity, dry spun experimental PAN homopolymer yarn and was not surface treated; a direct graphitization technique (i.e., no carbonization step) was used in the graphite fiber preparation. CS-3 is an experimental graphite fiber prepared from Villwyte rayon and was not surface treated. CS-5 is an experimental graphite fiber prepared from commercial PAN yarn, Dralon T (Farbenfabriken Bayer AG), by a catalytic direct graphitization

TABLE I

FIBERS STUDIED IN PROJECT

Fiber	Modulus, MSI	Strength, KSI
WYB	6	90
CS-2	41	329
Fortafil 5-Y	50	250
CS-4	88	341
CS-1	100	318
CS-3	104	409
CS-5	116	360

process (British specification 1,295,289, H. M. Ezekiel), and was not surface treated.

SECTION III

RESULTS AND DISCUSSION

Changes in the average structure with modulus are illustrated in Fig. 1, a montage of direct contact prints of Debye-Scherrer photographs of collimated fiber bundles of the fibers studied. Little evidence exists for any preferred orientation of the basal plane in WYB. Furthermore, no diffraction lines are present characteristic of three dimensional ordering. The relative lack of appreciable small angle scattering coupled with the low fiber density indicates very large porosity of relatively uniform size.

Diffractometer traces indicate that the average d_{002} for WYB is 3.42Å, very close to the pure turbostratic carbon, and the basal plane stack height (l_c) is only about 5-6 basal layers. Calculations of l_a were not performed because the proper evaluation is indeterminate when the material is primarily turbostratic. Overall then, the structure of WYB is poorly developed.

Increasing modulus is accompanied by a corresponding increase in preferred orientation as can be seen from the montage; the angular extent of the (0002) diffraction, ϕ, decreases.

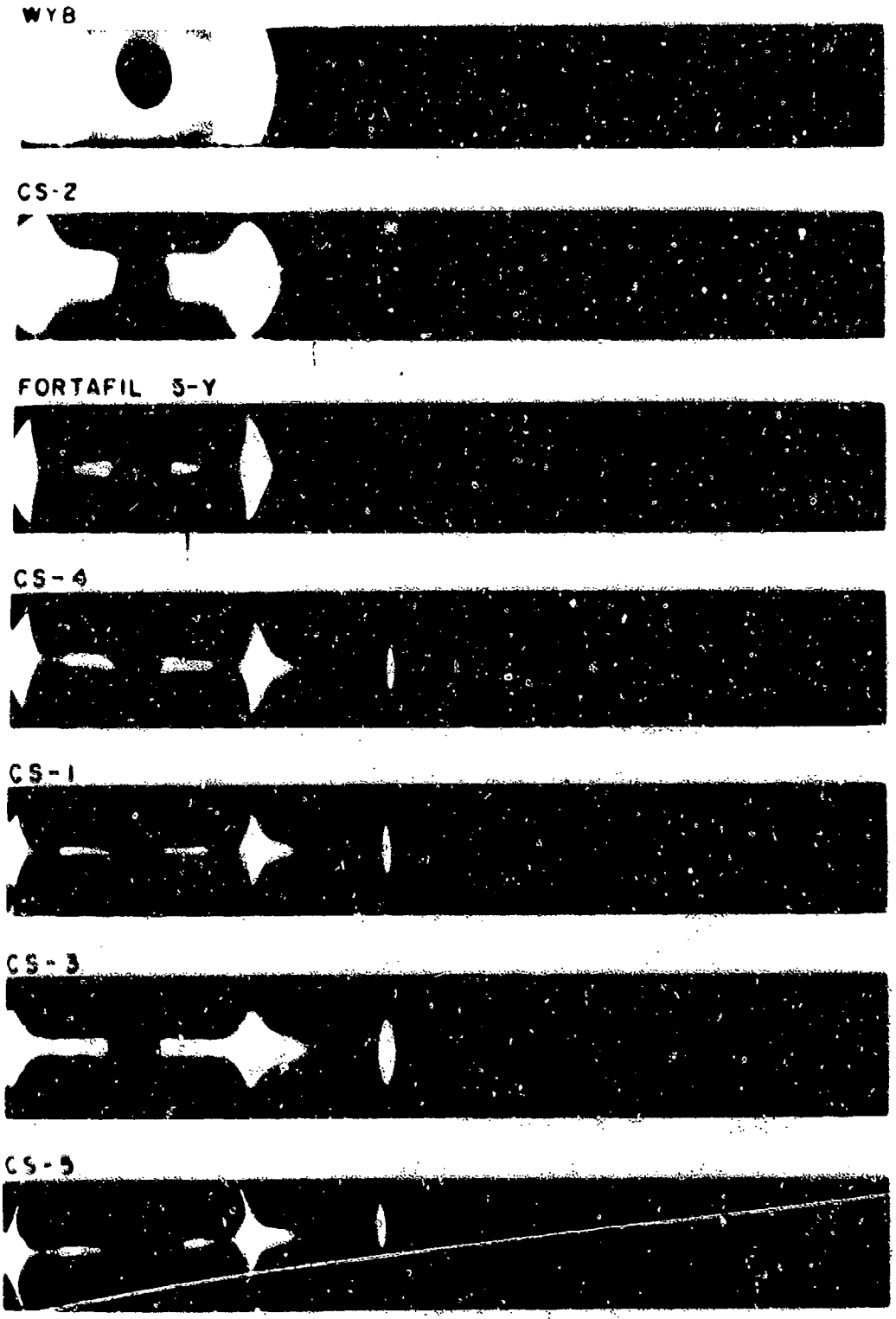

Fig. 1 Debye-Scherrer x-ray diffraction of fibers in order of increasing modulus (top to bottom).

This is quantitatively shown in Fig. 2, a plot of $W_{\frac{1}{2}}$, the uncorrected width at half maximum intensity of the (0002) peaks in the axial direction, versus modulus; the form is typical of results found to date by other workers [3].

It is noteworthy that three dimensional ordering occurred in two of the high modulus fibers although crystalline ordering does not appear to be a necessary step in the development of high modulus as is illustrated by CS-3. Furthermore, while the crystallite size along the C-axis direction generally increased with modulus, a relatively large crystallite size is apparently not necessary for high modulus. Hence, a high modulus might be developed without the decrease in shear properties normally associated with large crystallite size.

There does not appear to be any clear relationship between the strengths of the fibers and atomic properties as measured by x-ray diffraction. In fact, as shown in Fig. 3, strength and modulus are related only in a very ill-defined manner for the studied fibers.

1. Electron Diffraction

The development of surface structure with increasing fiber modulus can be followed, but in less detail, using electron diffraction techniques. Fig. 4 is a montage of electron diffraction patterns of the fibers studied arranged in order of increasing modulus. It is apparent that surface preferred orientation increases with fiber modulus as was the case for the average structure.

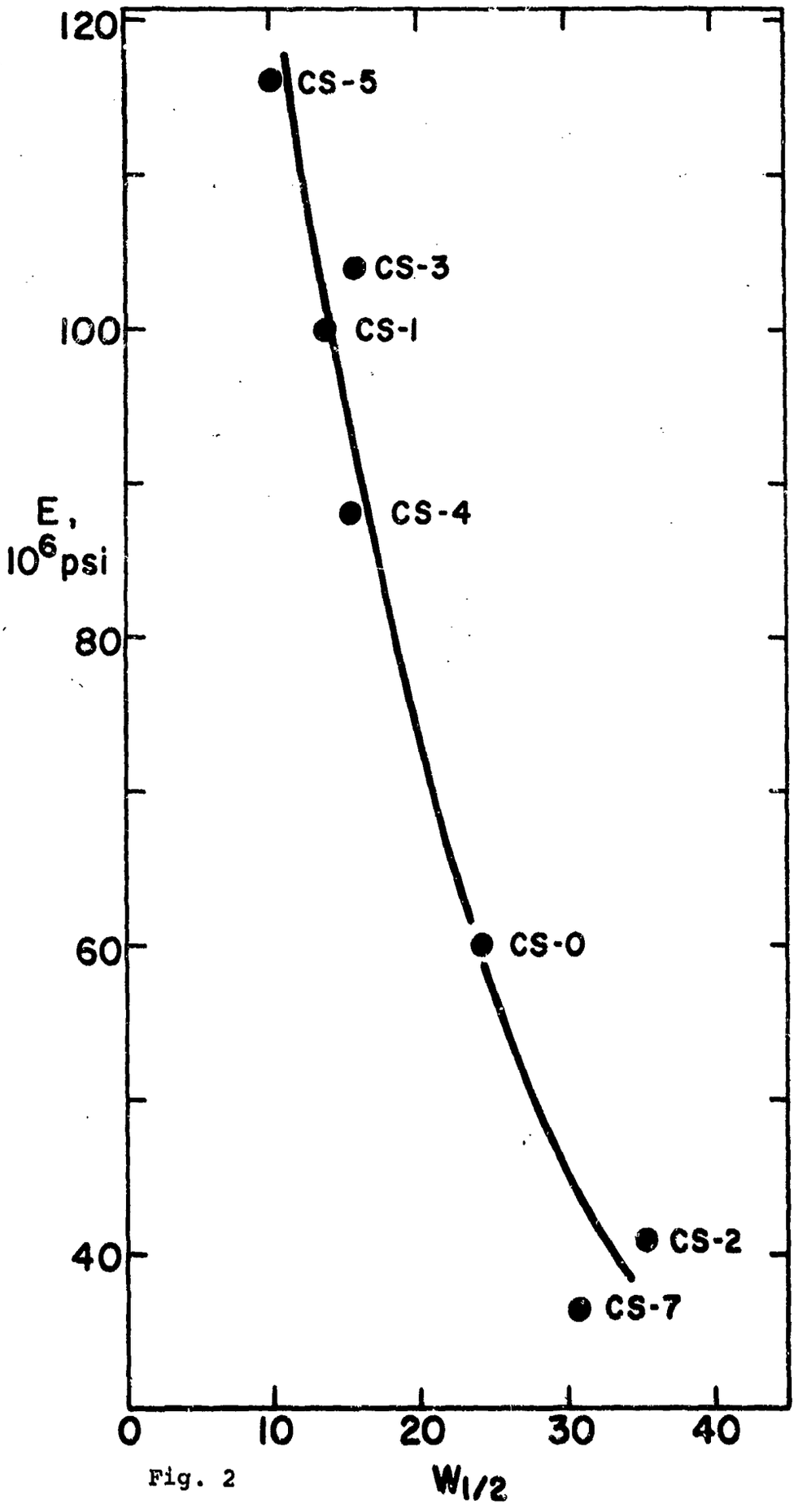
120
100
80
60
40
E,
10^6psi
CS-5
CS-3
CS-1
CS-4
CS-0
CS-2
CS-7
0
10
20
30
40
W1/2

Fig. 2

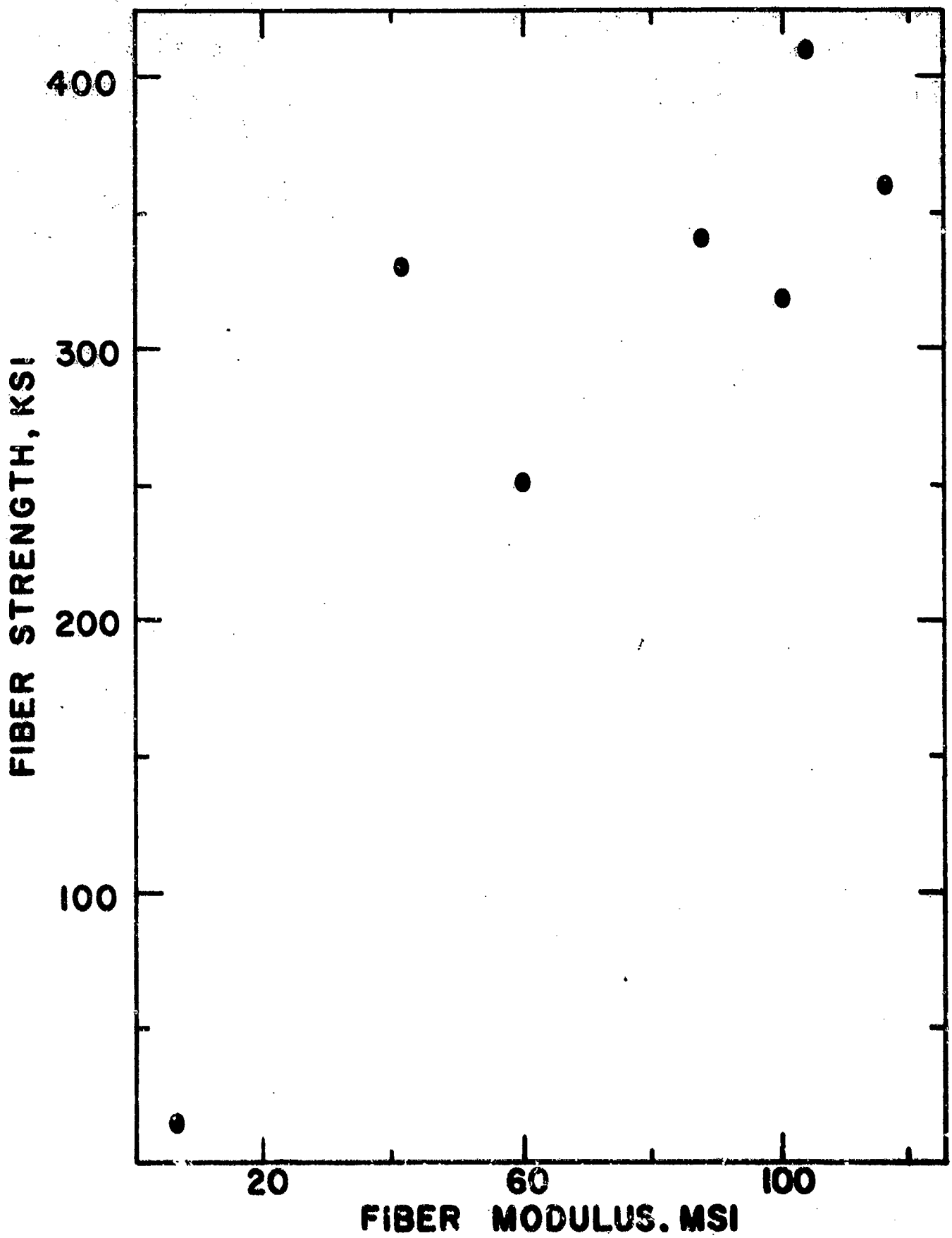

Fig. 3 Strength vs. modulus of fibers.

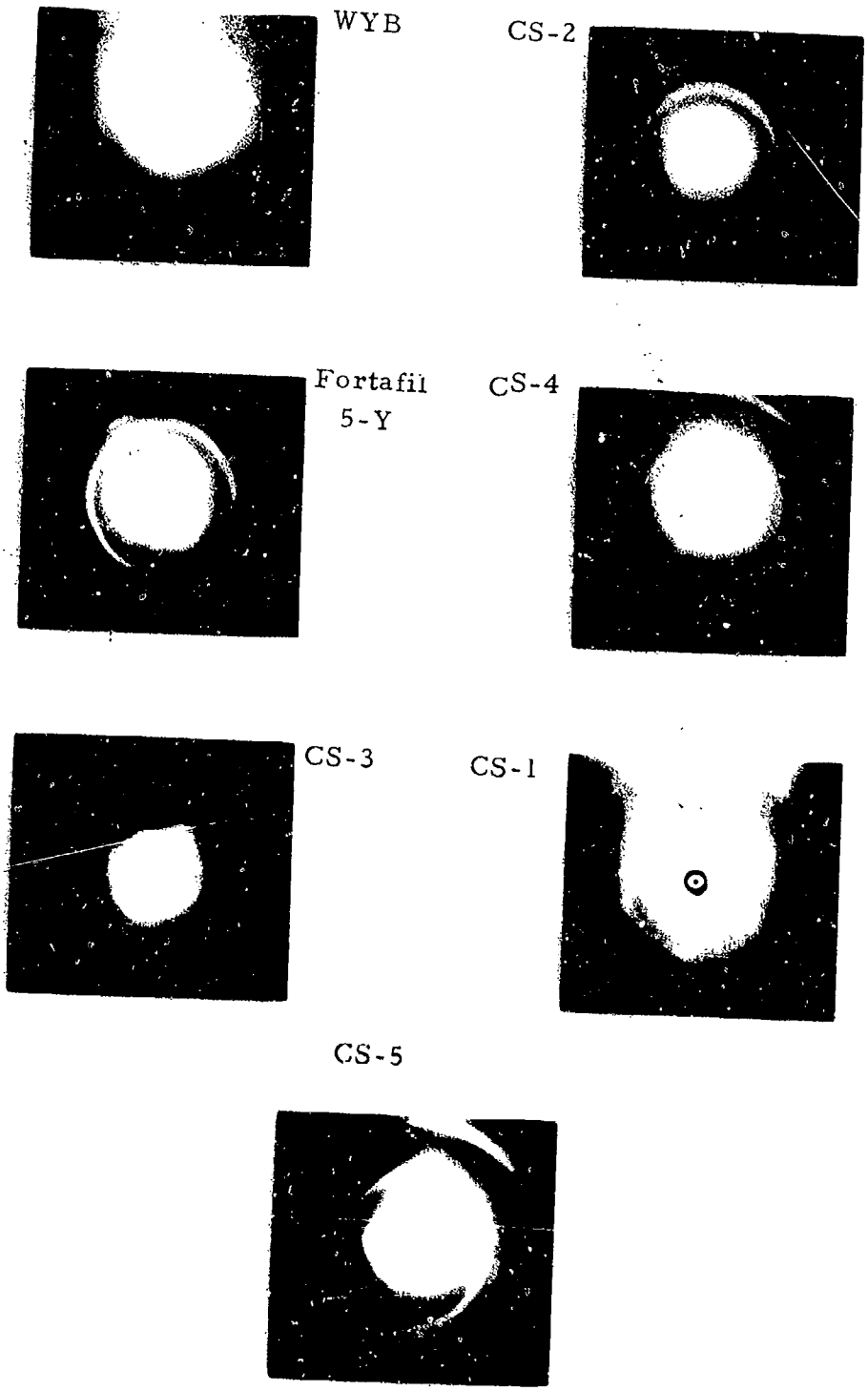

Fig. 6 Electron diffraction patterns of fibers in order of increasing fiber modulus.

Only in the case of CS-1 is the $(10\bar{1}0)$ band modulated into intensity maxima indicating that the a-axis possesses a preferred alignment. However, at this point in the structural development it is not clear whether the origin of the $(10\bar{1}0)$ and the (0002) maxima are ultrastructurally the same.

2. Electron Microscopy

With increasing modulus other changes, in addition to increased preferred orientation, are observed in fiber structures. As just described, a higher modulus fiber is in general characterized by a better aligned axial structure, and it might therefore be expected that more crack deflection mechanisms would be operable parallel to the fiber axis. By contrast, a low modulus fiber would fracture more like a brittle equiaxed grained polycrystalline metal bar. The evidence supports this supposition. Fig. 5 is a montage of the profiles of various fibers broken in bending taken in bright field with the electron microscope. As the modulus increases there is a progressive change from a blunt to a very jagged fracture profile.

More information about surface structure is obtainable using replication techniques. It would be expected that higher heat treatments would impart a more graphitic nature to fiber surfaces and observed textures would be expected to change. Furthermore, surface treatment effects would probably change the surface character. Fig. 6 is a montage of replicas of fibers studied; it is significant that the higher modulus fibers possess a relatively

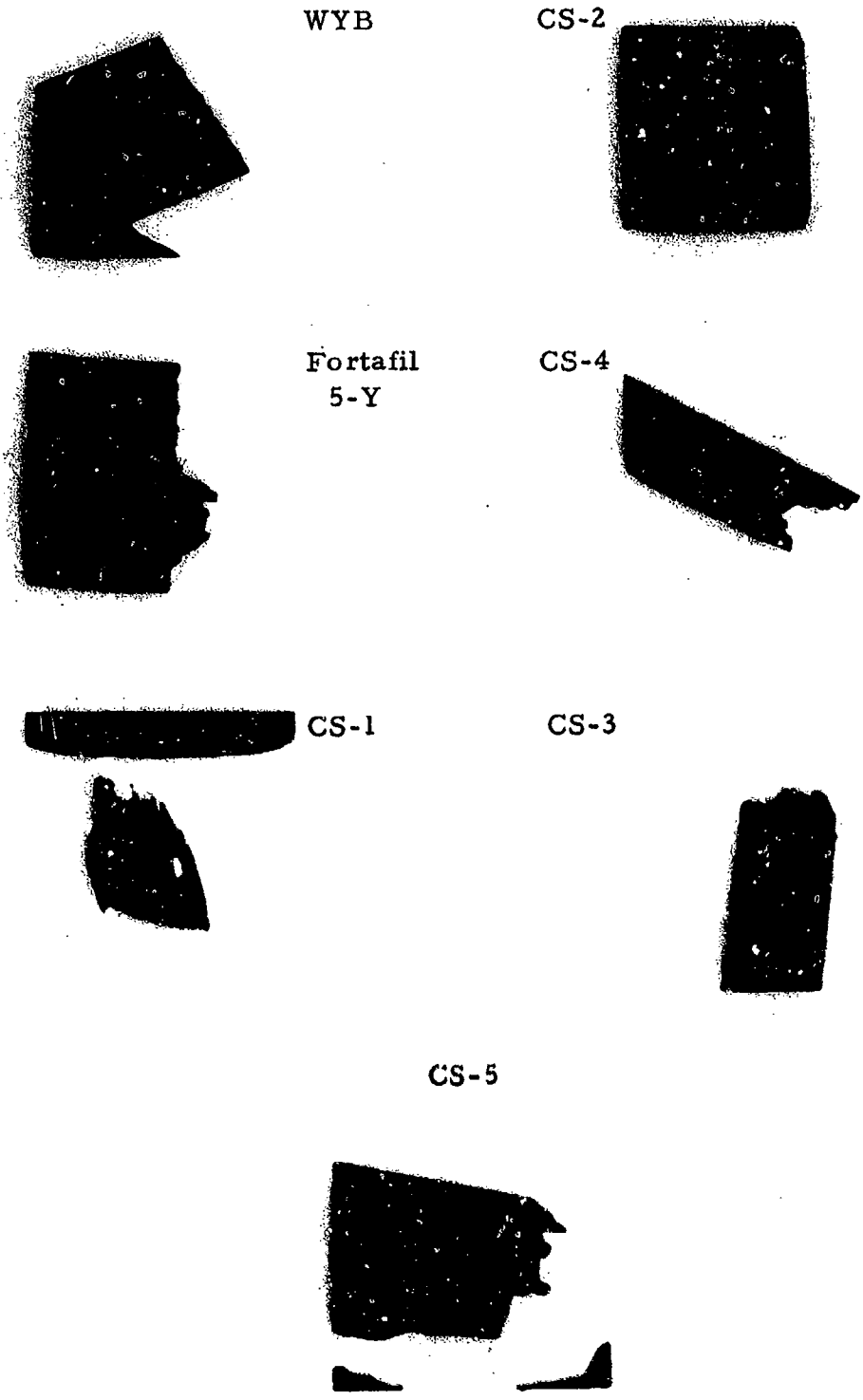

Fig. 5 Bright field fracture profiles of fibers in order of increasing modulus, 1 cm ≈ 2.5μ.

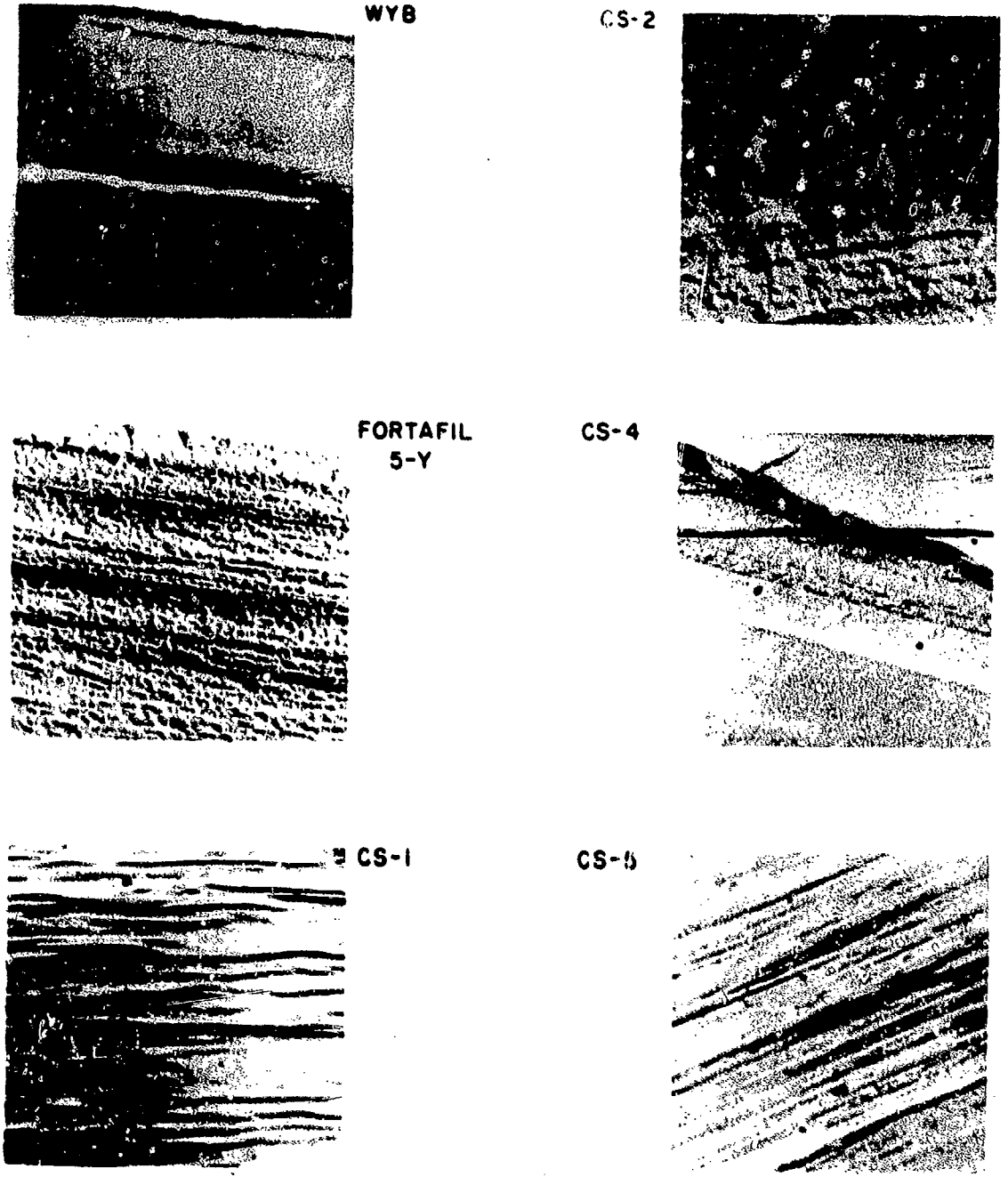

Fig. 6 Replicas of longitudinal surfaces of fibers in order of increasing modulus, 1 cm ≈ 0.70μ.

smooth and rippled surface reminiscent of pyrolytic graphite, while the low strength fibers are rougher. Note that the sample of Fortafil 5-Y, surface treated, has about the same roughness as lower modulus fibers. It is apparent that a surface treatment which etched the fiber surface, as here, would improve the shear properties of the composite parallel to the fiber lay-up. On the other hand the highly basal and smooth surfaces of the untreated high modulus fibers would be difficult to wet and consequently low composite shear properties would be anticipated.

3. Dark Field Electron Microscopy

The progression from low to high modulus in fibers is further illustrated by changes in the ultrastructure which has been elucidated in the fibers studied, using the dark field technique. Fig. 7 is a (0002) dark field photograph of the fractured end of a 41 million modulus fiber. Note that very little diffraction contrast is observed either along the side of the fiber or at the end (blocked area). Little else is observed even at significantly higher magnifications. Contrast this with an analogous (0002) dark field of a fractured end of a 50 million modulus fiber, Fortafil 5-Y, in Fig. 8. Distinct diffraction reflections over areas about 100Å in diameter are evident. However, it is apparent that the diffracting areas bear a relationship to each other; they appear to be part of a ribbon-like structure parallel to the fiber axis. The length of the ribbons are of the order of thousands of angstroms

Fig. 7 (000?) Dark field, CS=2, 1 cm = [illegible].

Fig. 8 (0002) dark field, Portafil 5-V, 1 cm ≈ 650Å.

or more, although the diffracting volumes are about 100Å on a side. The inconsistencies in l_a crystallite measurements, and the long ribbon structure can be removed by assuming that the ribbons have a ripple. Close inspection of Fig. 8 reveals that a rippled ribbon could be present. This was verified by taking electron photographs of the same fiber area at different positions of the electron microscope's objective aperature over the (0002) diffraction ellipse. Superposition of the negatives showed the total morphology of the structures to be rippled ribbons.

A thin fractured section (0002) dark field photograph of the 100 million modulus fiber, CS-1, is illustrated in Fig. 9. The ribbons are straighter, and a remarkable correspondence of diffracting areas perpendicular to the fiber axis exists. This probably indicates first stages of ribbon fusion perpendicular to the fiber axis.

The dark field analysis of CS-1 could be developed more because of its more highly developed crystal structure. An electron diffraction pattern of CS-1 is illustrated again in Fig. 10. Distinct $(10\bar{1}0)$ intensity maxima appear implying that their atomic planes are aligned with each other. The relationship of these $(10\bar{1}0)$ maxima to the (0002) ellipse implies the structure is as illustrated in ribbon 1 rather than ribbon 2 in Fig. 11. The $(10\bar{1}0)$ dark field is shown in Fig. 12; the long ribbon-like structure is again apparent.

Fig. 9 (0002) dark field, CS-1, 1 cm ≈ 740Å.

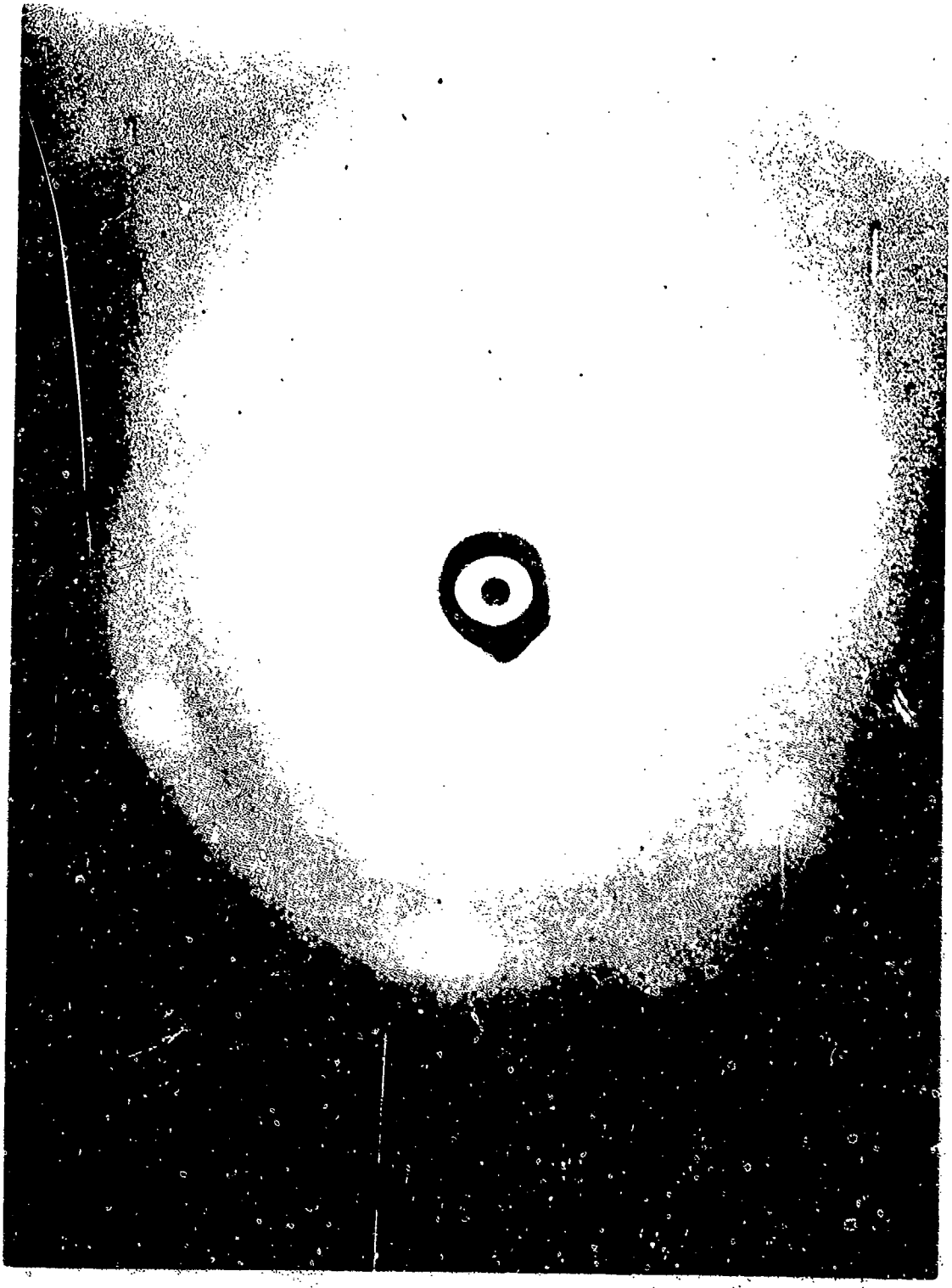

Fig. 10 Electron diffraction pattern, CS-1.

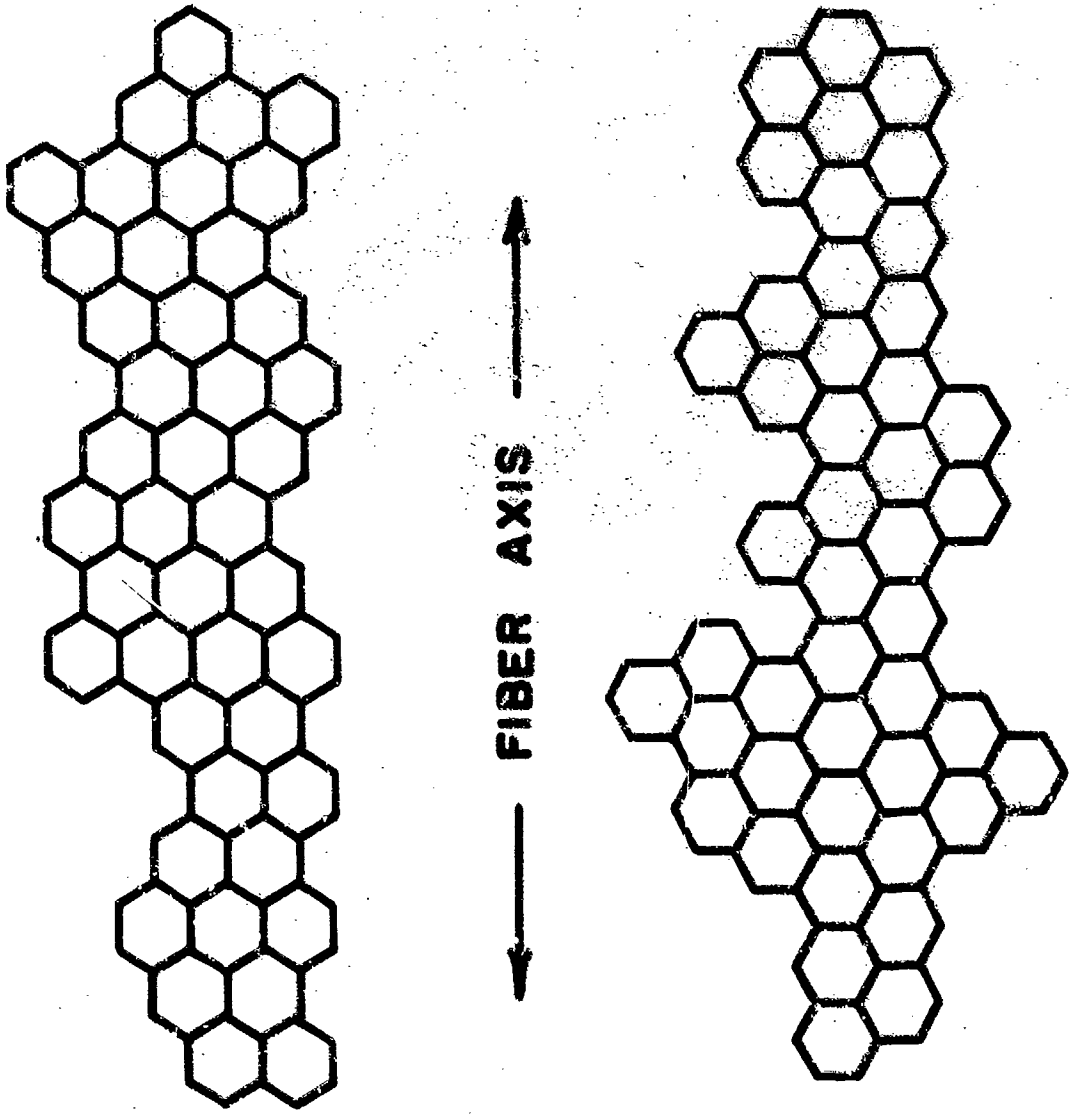

Fig. 11 Schematic representation of the orientation of carbon rings within the ribbon structure of a section of a CS-1 fiber.

Fig. 12 $(10\bar{1}0)$ dark field, $\vec{g}=\vec{1}$, 1 cm = 700A.

While only the dark fields of three fibers have been specifically mentioned here, it is evident that the general trend is for longer, larger, and particularly straighter microfibrils as modulus increases. Fracture tends to occur along the ribbons giving rise to the jagged profiles alluded to before.

4. Scanning Electron Microscopy (SEM)

The results described so far, with the exception of the surface replicas, give information which essentially describes axial structures. Nothing has been said about the overall shapes of fibers, fracture patterns, or radial structural distributions. Magnifications necessary to obtain usefully high resolutions of the fibers and their textures are outside of optical capability; SEM provides such capacity.

Fig. 13 is a SEM photograph of WYB fractured in bending in an epoxy matrix. The irregular rayon base shape is apparent as is the rather flat or blunt fracture surface.

Fig. 14 is a SEM photograph of ends of Fortafil 5-Y similarly fractured. From the end fracture pattern it appears that the cross-sectional structure may be similar to that shown schematically in Fig. 15. Here the dashed lines represent the edges of basal planes arranged with centrosymmetry with respect to the fiber axis. This particular structural scheme is significant in that appreciable residual stresses would be generated upon cool down from processing temperature. This is caused by the anisotropy in thermal expansion

Fig. [illegible] A scanning electron micrograph of [illegible] fracture surface in an epoxy matrix. [illegible] μm.

Fig. 14 Scanning electron micrograph of Fortafil 5-Y fibers fractured in bending in an epoxy matrix. 1 cm ≈ 2.0μ.

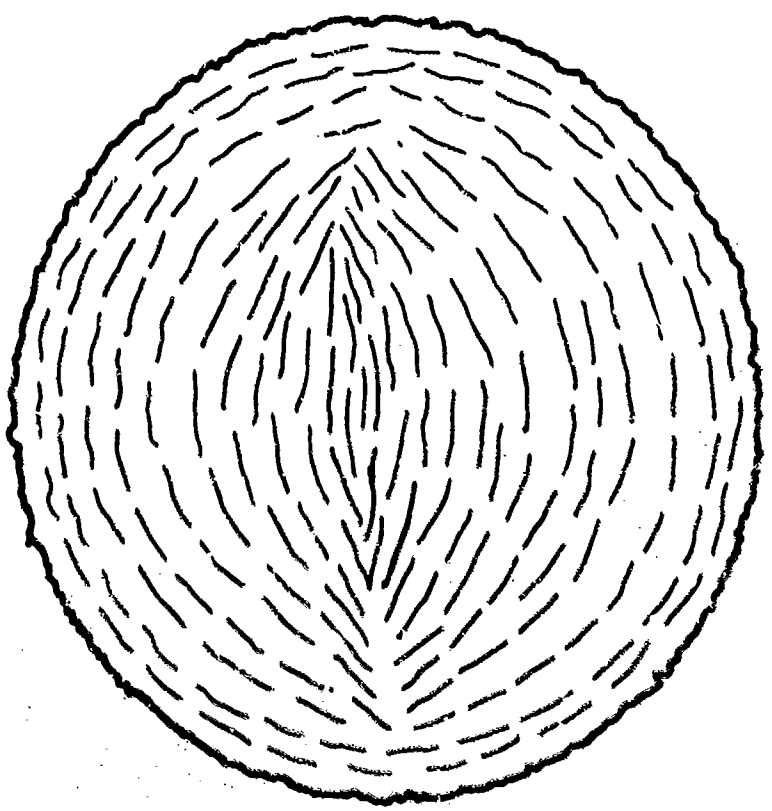

Fig. 15 Radial preferred orientation texture from preceding scanning electron micrograph.

coefficient and the effect would become more acute with higher processing temperatures since the radial preferred orientation is increased and the temperature difference greater. This would be expected to change the fiber fracture pattern and decrease the tensile strength.

Also, from the photograph, the surface roughness of the longitudinal fiber surface first described from the carbon extraction replica is verified.

One final example of radial structural development using SEM is in the 100 million modulus fiber, CS-1, shown in Fig. 16. The dog-bone shape is apparent. Also the resolution is somewhat better here and it appears as though a higher fraction of the basal planes are parallel to the fiber axis, and that the radial alignment bears some relation to the external shape.

Thus, with increasing modulus, it becomes apparent that the radial distribution develops along with the axial, although the exact nature of the development is not strictly determinable from SEM since the fracture patterns may only be related to actual radial structures. A potentially more reliable technique is polarized light microscopy to be discussed later.

5. Fiber Etching Using Reverse Radio Frequency Sputtering

One of the reasons for developing an acceptable etching procedure is for use in reflected polarized light microscopy, i.e., radial preferred orientation may be distorted in typical polishing

Fig. 16 Scanning electron micrograph of CS-1 fiber fractured in bending in an epoxy matrix, 1 cm ≈ 0.40μ.

procedures. Most highly graphitic fibers might be expected to smear easily.

Various techniques have been used in attempts to progressively remove limited amounts of carbon fiber surface so that interior structure may be directly observed. Typical etching procedures have included chemical methods and flame polishing (air oxidation). While useful results have been obtained, these techniques may possibly damage surface structure to the point of being non-representative, particularly on a micro to ultra scale. For this reason and because controlled amounts of etching was desired, radio-frequency (R.F.) sputtering of various carbon fibers mounted in epoxy matrices was investigated. Fig. 17 is a SEM photograph of 100 million modulus CS-1 fibers fractured in bending in an epoxy matrix before the R.F. sputter. Fig. 18 is the same sample after the section was mechanically polished and then sputter etched in N_2 gas. Optical filar measurements revealed that average fiber cross-sectional dimensions decreased by one to two microns and that the epoxy matrix was simultaneously etched back 10 to 20 microns after a one-hour sputter. This etch revealed that a stringy texture exists below the surface, far different from CS-1 surfaces seen to date. The pitted end is an indication of structural inhomogeneity, or perhaps due to the overall poorer microfibrillar coupling expected in such a high performance fiber.

The same reverse sputtering procedures were tried with Portafil

Fig. 17 Scanning electron micrograph of CS-1 fibers fractured in bending in an epoxy matrix, 1 cm ≈ 2.0μ.

Fig. 18 Scanning electron micrograph of a different area of the sample shown in Fig. 17 after polishing and RF reverse sputter etching, 1 cm = 1.0μ.

5-Y. Fig. 19 is a replica of an end of one of these fibers. The blocked area is shown at higher magnification in Fig. 20. Structural relief parallel to the fiber axis is again apparent, but the texture is markedly different from CS-1. Close inspection of this figure gives indications of structural units about 100Å thick (steps) stacked parallel to the fiber axis. Notice however, that the end of the fiber has been polished smooth rather than pitted as in CS-1. This may be an indication of better microfibrillar coupling, i.e., due to poorer axial development.

One final example of information obtained from fiber etching using reverse sputtering is with the 116 million modulus fiber, CS-5. Shown in Fig. 21 is a SEM photograph of the ends of CS-5 fibers fractured in an epoxy matrix. From the fracture pattern the radial structure appears to be similar to that shown in Fig. 22. Reverse sputtering under the standard conditions produced the results shown in Fig. 23. It appears that CS-5 fibers etch as though they were composed of several layers; an outside layer of high axial alignment, a core of lower development perhaps like Fortafil 5-Y, and a narrow but well defined intermediate region. This multiple structure may explain the apparently anomalous low preferred orientation indicated by the x-ray Debye-Scherrer photograph of CS-5.

6. Reflected Polarized Light Microscopy

Because carbonaceous materials possess high absorption coefficients in the visible spectrum, optical techniques of transmission microscopy are difficult. The practical obstacles in the case of

Fig. 19 Replica of the end of a Portafil S-Y fiber which was polished and RF reverse sputter etched, 1 cm ≈ 0.30μ.

Fig. 20 Blocked area in Fig. 19 shown at high magnification, 1 cm ≈ 1200Å.

Fig. 21 Scanning electron micrograph of GS-S fibers fractured in an epoxy matrix, 1 cm = 2.5μ.

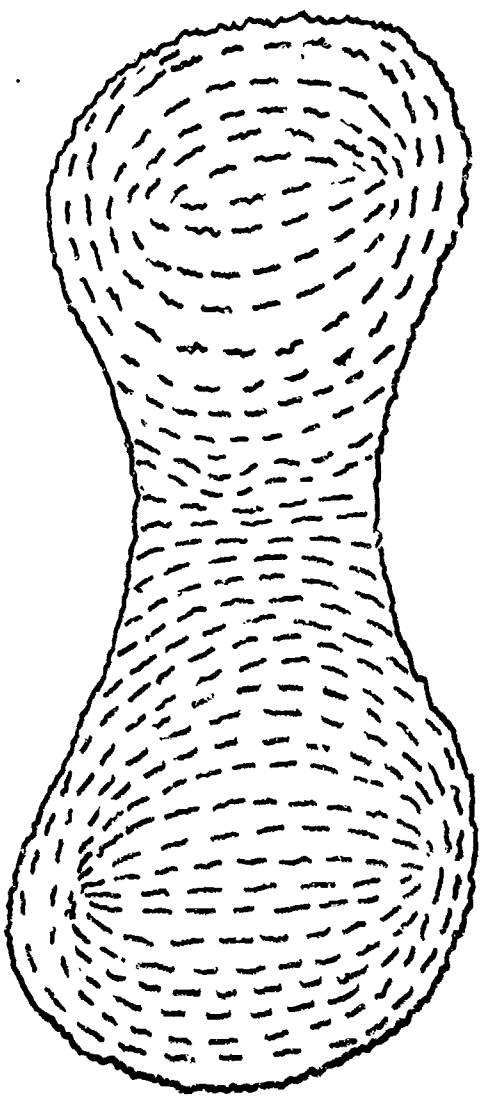

Fig. 22 Schematic of radial preferred orientation texture from Fig. 21.

Fig. 23 Scanning electron micrograph of a different area of the sample shown in Fig. 21 after polishing and RF sputter etching. 1 cm = 4.0μ.

carbon fibers are much more formidable due to the problem of obtaining an undistorted cross-section intact and not much more than several hundred angstroms in thickness. A reflected polarized light analysis is thus more attractive. Given in Appendix II is a development of optical theory permitting semi-quantitative determinations of the radial distributions in fibers.

However, even if practical considerations do not easily permit semi-quantitative results to be obtained, it is possible in many cases to at least show qualitative development of radial structure with increasing modulus. Figs. 24 and 25 are montages of reflected polarized light photographs of rayon base fibers. The lowest modulus fiber, WYB, is totally extinct with the exception of a thin fringe of optical activity on the outside surface; this is probably due to relief polishing. The total and uniform extinction indicates either a random radial distribution, some sort of symmetric radial distribution but the basal planes intersect the surface at $\phi \sim 30°$, or both. Whatever the situation, the structure is poorly developed relative to Thornels 25 and 50 where more optical activity accompanies increasing modulus. The 104 million modulus fiber CS-3, is seen to consist of two types of fibers; it is probable that the larger, uniformly dark fibers broke during stretching and have an anomalously low structural development.

Fig. 26 is a montage of optical micrographs of the 41 million modulus fibers, CS-2. The "Formeé Cross of Heraldry" pattern is

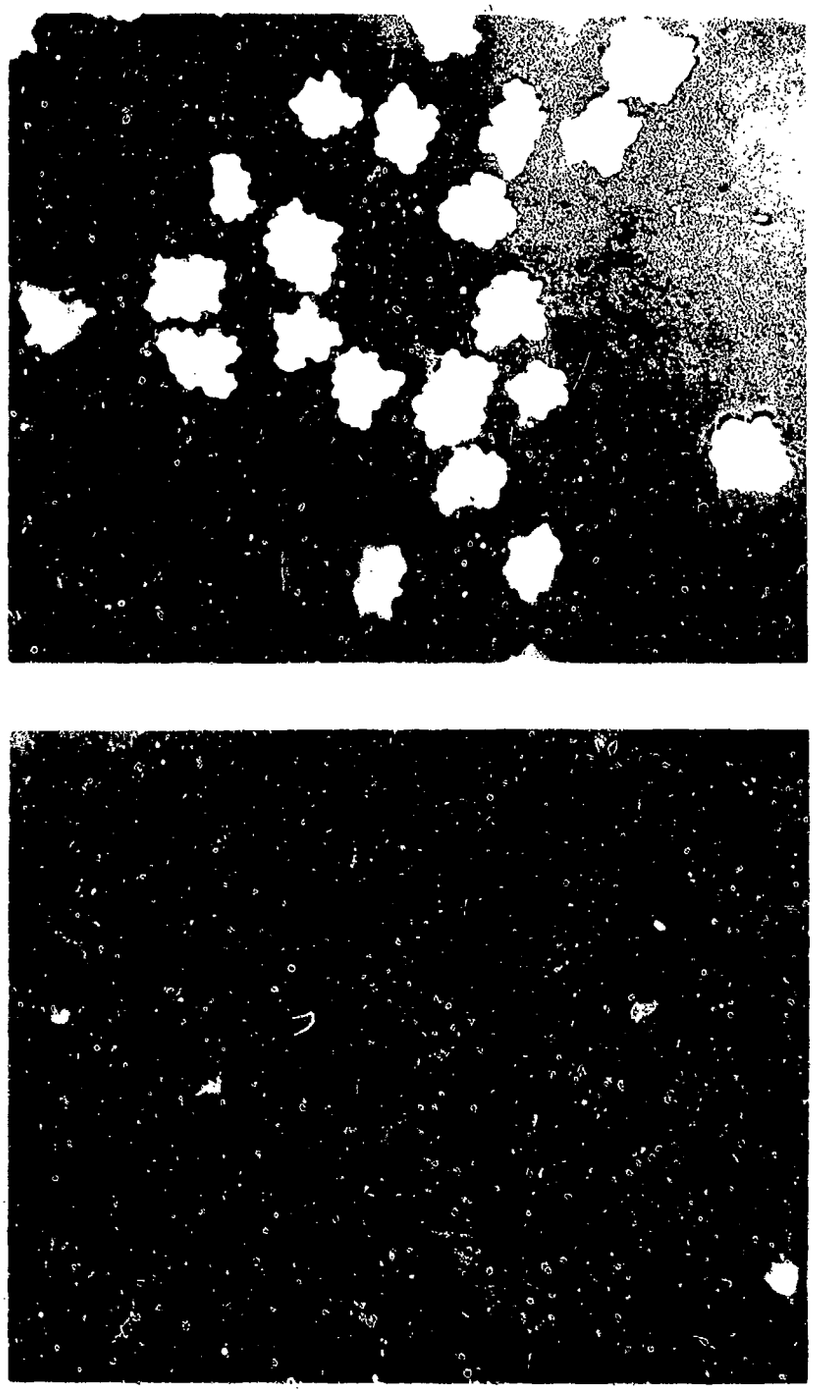

(a)

(b)

Fig. 24 Polished cross section of WYB fibers mounted in an epoxy matrix: a) plane light, b) polarized light, 1 cm ~ 7.5μ.

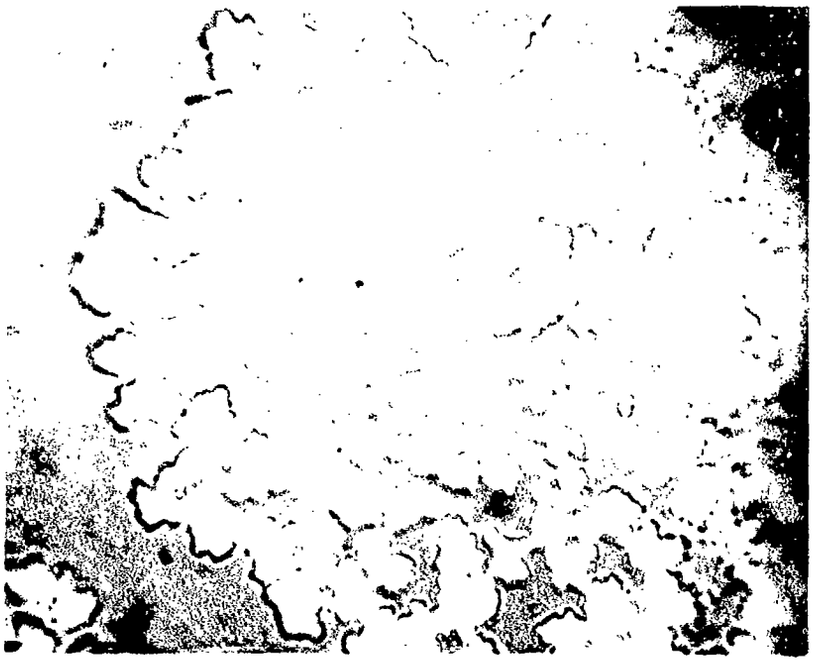

(a)

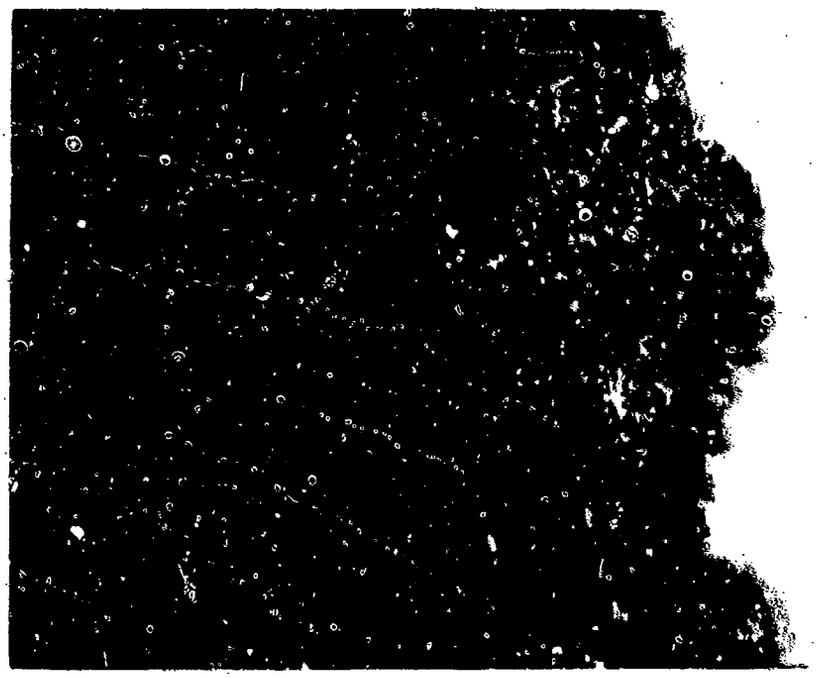

(b)

Fig. 25 Polished cross section of CS-3 fibers mounted in an epoxy matrix; a) plane light, b) polarized light, 1 cm · 7.5μ.

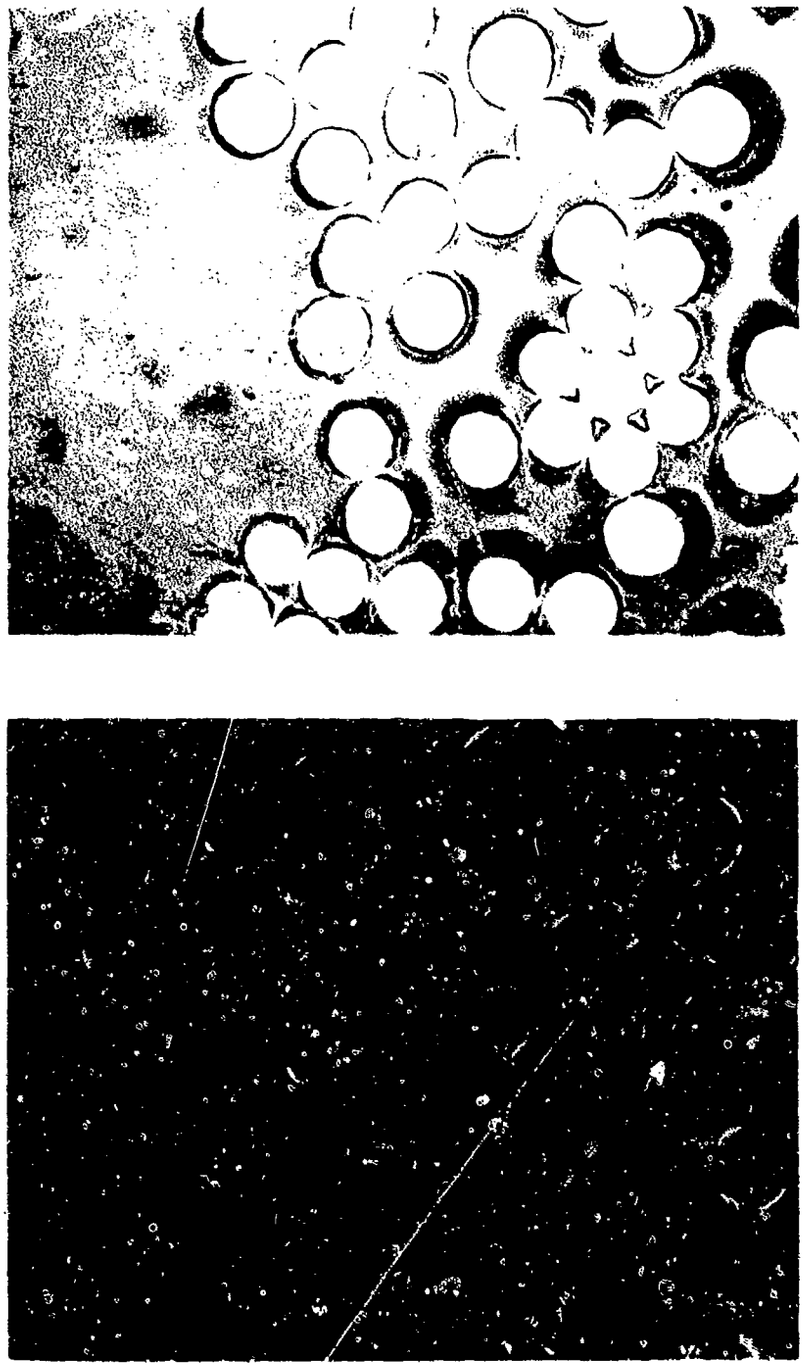

(a)

(b)

Fig. 26 Polished cross section of CS-2 fibers mounted in an epoxy matrix; a) plane light, b) polarized light, 1 cm ≈ 7.5μ.

clearly seen in the polarized light photograph. The behavior of the isogyres indicates that this fiber has a primarily "tree trunk" radial motif; a maximum value of A_R of 8-10° measured at the circular perimeter implies that ϕ near the fiber surface is about 10° with respect to the fiber axis, poorer alignment occurring in the fiber interior.

In Fig. 27, a montage of micrographs of Fortafil 5-Y, more complicated behavior is shown. In a number of these fibers optically determined tree trunk structures are observed and rotation angles of 12-14° have been measured at the outer surfaces. This implies better preferred orientation than the 41 million modulus fiber with ϕ being about 8°.

SECTION IV

THREE DIMENSIONAL MODELS OF FIBERS STUDIED

Synthesis of the techniques described and the results obtained enable three dimensional models of the fibers to be constructed. The fibers are characterized in order of increasing modulus.

The following schematic models are not drawn to scale in order to emphasize structural trends in single three dimensional representations. Fiber end fracture morphology and longitudinal surface roughness are shown at one magnification (≈ 10,000X), while the cut-away section is illustrated at about 100,000X. Possible gradations in axial preferred orientations from the surface to core of fibers are indicated purposefully, though it should be realized

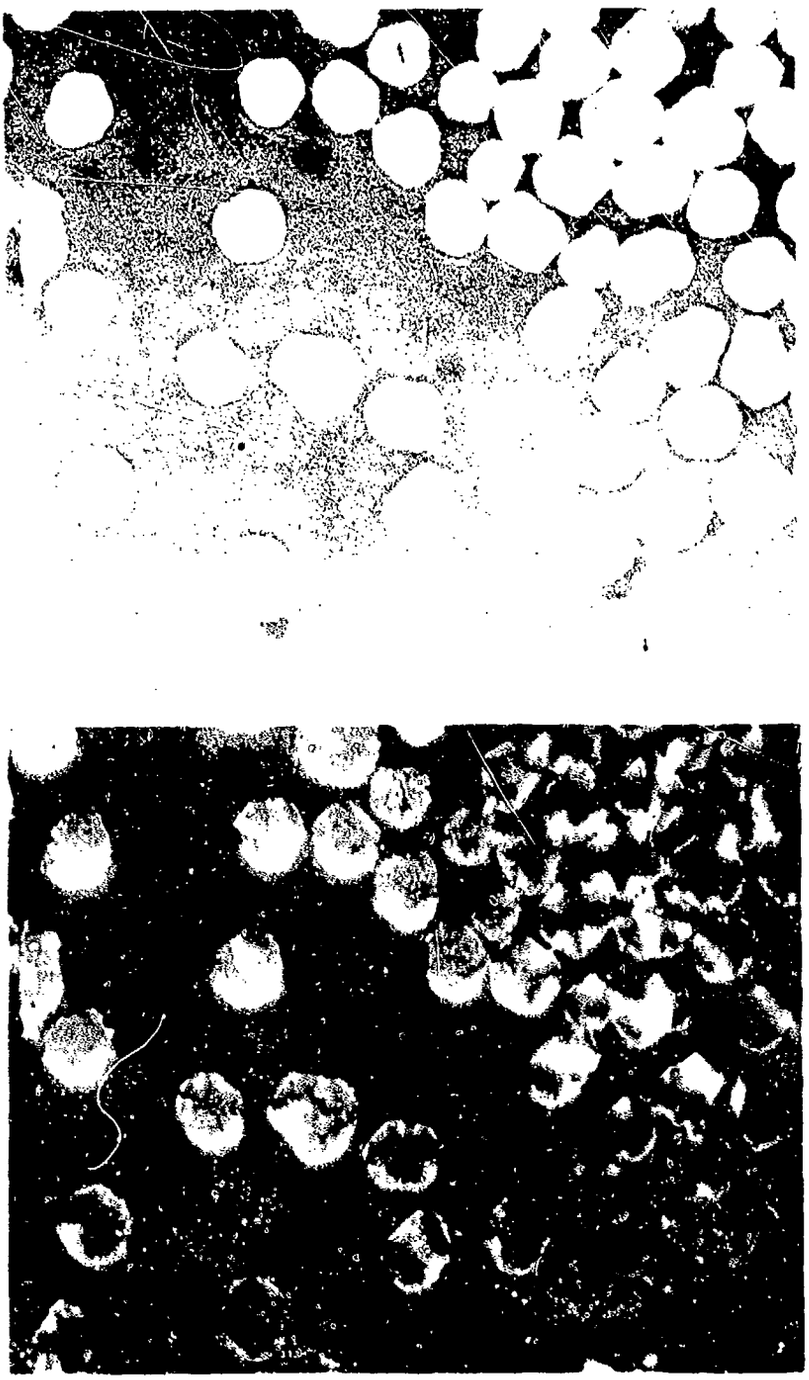

(a)

(b)

Fig. 27 Polished cross section of 5-Y fibers mounted in an epoxy matrix; a) plane light, b) polarized light, 1 cm ≈ 7.5μ.

that the numbers of basal layers shown is several orders of magnitude smaller than in the actual fiber from outside to center.

1. WYB, $E = 6 \times 10^6$ psi.

Fig. 28 is a schematic perspective drawing of a cut-away sector of a WYB fiber. From optical and SEM photos the irregular cross-sectional shape is established. Replicas and SEM confirm that the longitudinal surface is exceedingly rough as would be expected. Being the unstretched parent material of the Thornel Series, relatively little structural development is expected. In fact results from diffractometer traces indicate that the average d_{002} is 3.42Å; thus, WYB is essentially turbostratic with a small l_c of 18Å. In the series studied, its preferred orientation is the lowest; $W_{\frac{1}{2}}$, the angular width of the (0002) peak at half maximum intensity, is 69°. Extrapolation back from dark field photographs of higher modulus fibers leads to an axial structure consisting of relatively short microfibrils oriented at all angles to the fiber axis with a high amplitude to wavelength ratio. The flat fracture profiles suggests the coupling between adjacent microfibrils is large, or perhaps the ribbons are extensively tangled. Finally, the results from optical studies and fracture patterns, seen using the SEM indicate little or no radial preferred orientation.

2. CS-2, $E = 41 \times 10^6$ psi.

Fig. 29 is an analogous schematic perspective drawing of the structure of CS-2. This fiber has a circular cross-section and its

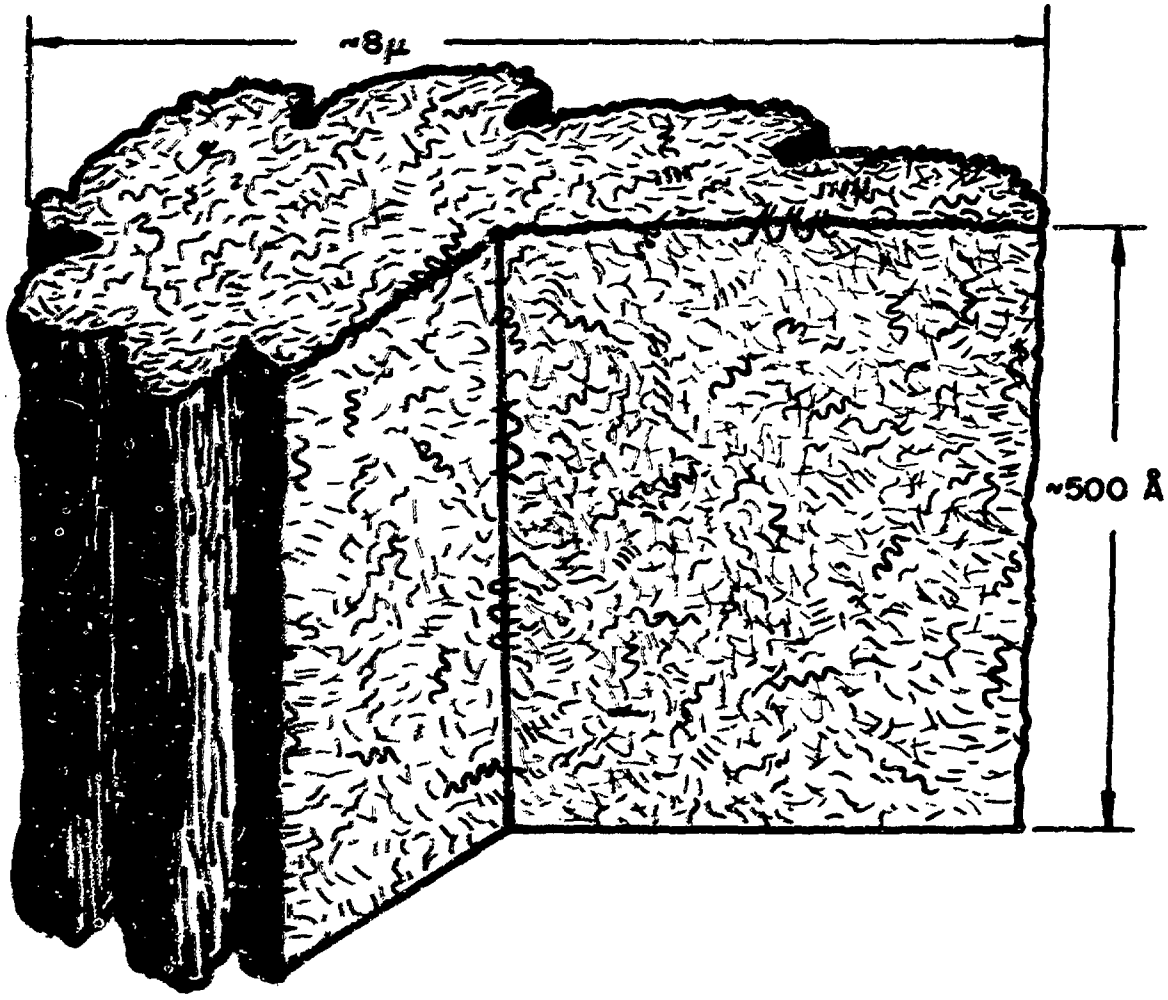

Fig. 28 Schematic 3-D structural model of WYB.

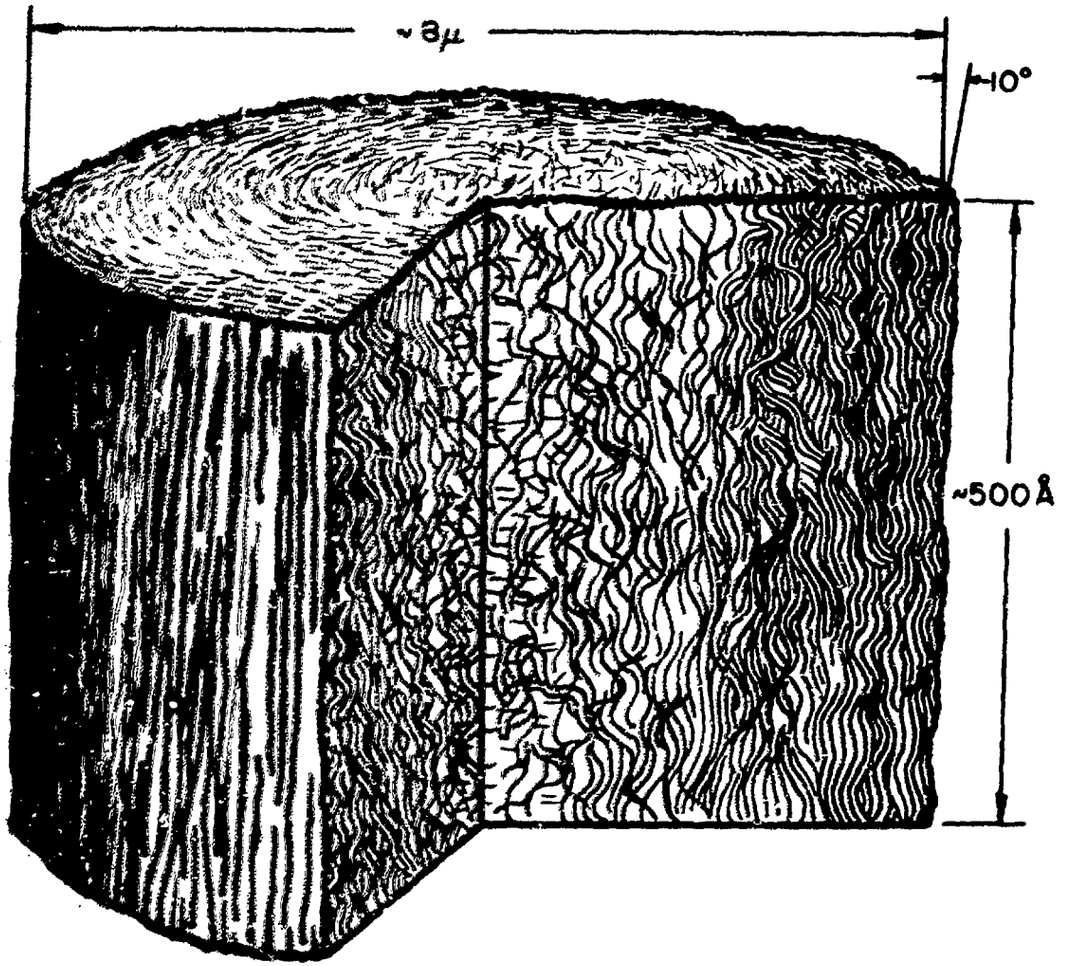

Fig. 29 Schematic 3-D structural model of CS-2.

longitudinal surface is fairly rough, but this is probably due to surface treatment. The average basal spacing is 3.42Å, and l_c is 16Å, both almost identical to WYB. However, a $W_{\frac{1}{2}}$ of 35° indicates better average axial preferred orientation. A maximum value of the optical extinction angle of 10° at the fiber surface indicates that $\phi \approx 10°$ there. The behavior of the isogyres suggests the radial distribution is "tree trunk" and more highly aligned near the outer surface. The "tree trunk" model is also supported by a circumferential fracture pattern seen in SEM. A blunt fracture profile infers relatively good radial basal coupling. The ratio of microfibril amplitude to wave length is less than in the case of WYB, and the ribbons are longer.

3. Fortafil 5-Y, $E = 50 \times 10^6$ psi.

The cross-sectional shape of Fortafil 5-Y is approximately circular, and the longitudinal surface has been roughened by surface treatment as shown schematically in Fig. 30. An average d_{002} of 3.37 and l_c of 100Å indicates a much better developed layer structure having a $W_{\frac{1}{2}}$ of 24°. Dark field photographs indicate larger l_c values at the surface. The ribbon morphology is clearly established with ribbon lengths extending into the micron range; the amplitude to wavelength ratio is less than unity. The irregular fracture pattern indicates crack deflection fracture mechanism operation. The radial structure is "tree trunk", at least near the outer surface where ϕ is about 8°; the interior radial structure is

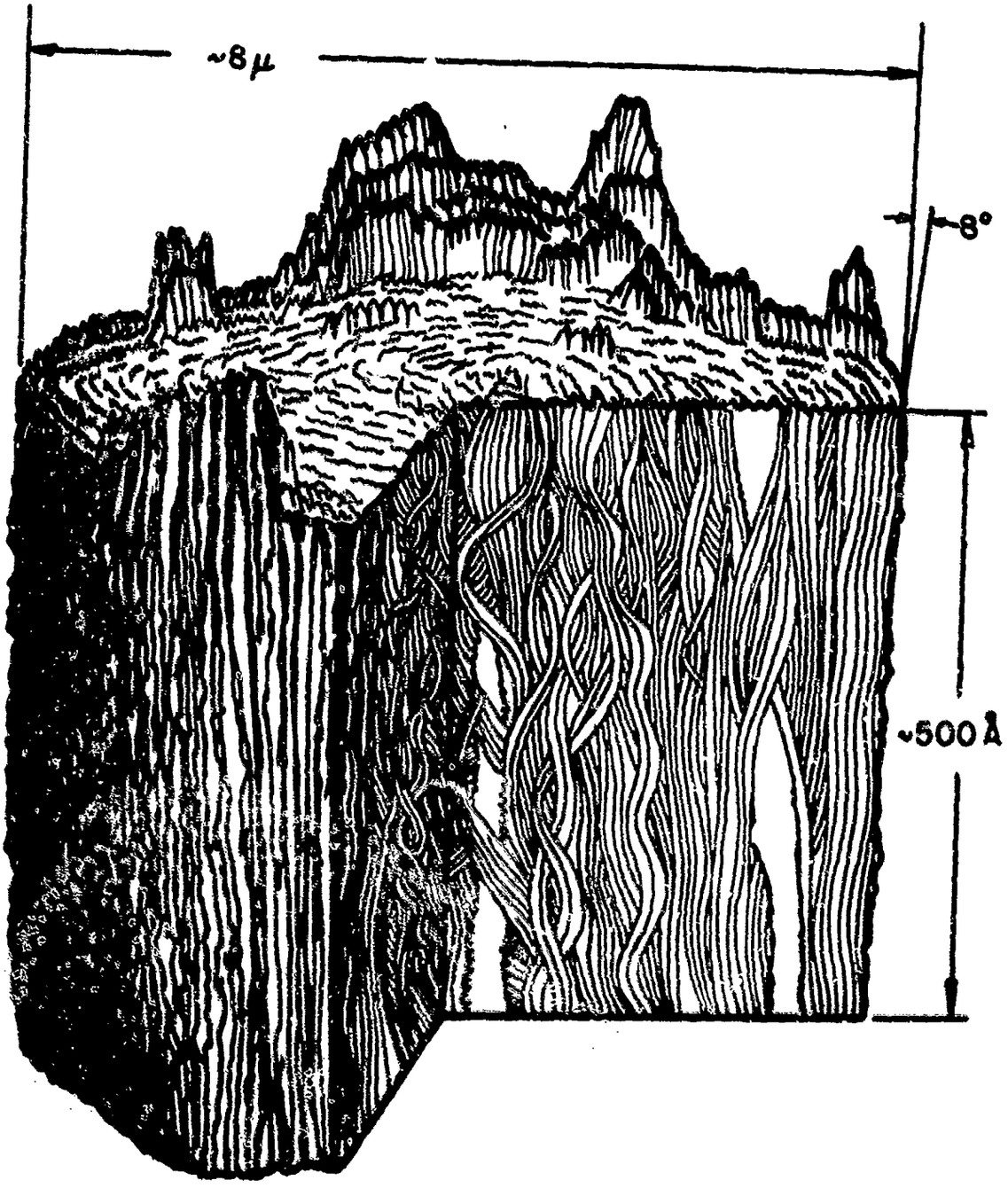

Fig. 30 Schematic 3-D structural model of S-Y.

more complex and less aligned.

4. <u>CS-4, E = 88 x 10^6 psi</u>.

CS-4, Fig. 31, is a rayon base fiber with a well developed axial structure. From x-ray data the average d_{002} is 3.37Å and l_c is 155Å; preferred orientation is still better than Fortafil 5-Y with $W_{\frac{1}{2}}$ being 16°. The relatively large l_c may be related to the catalytic graphitization procedure. The microfibrils are poorly coupled; in some (0002) dark field photographs continuous ribbons 3μ in length are present. Optically, CS-4 is complex, but SEM of fractured ends suggests a centrosymmetric radial structure with layer planes parallel to the fiber surface.

5. <u>CS-1, E = 100 x 10^6 psi</u>.

CS-1, Fig. 32, has a dog-bone shape and is the most graphitic of the fibers studied with a d_{002} of 3.36Å, an l_c of 180Å, and $W_{\frac{1}{2}}$ of 14°; significantly, three dimensional lines are present in its Debye-Scherrer pattern. The surface is locally very smooth and rippled, but SEM results indicate some overall roughness. The basal ribbons are very straight and long, and dark field results suggest that neighboring diffracting areas are cross-correlated inferring the first stages of ribbon fusion. Not only is a high degree of basal preferred orientation present, but there is a correlation of the l_a direction and the fiber axis. Radially CS-1 is also complex, but SEM and optical results indicate the surface is basically onion skin.

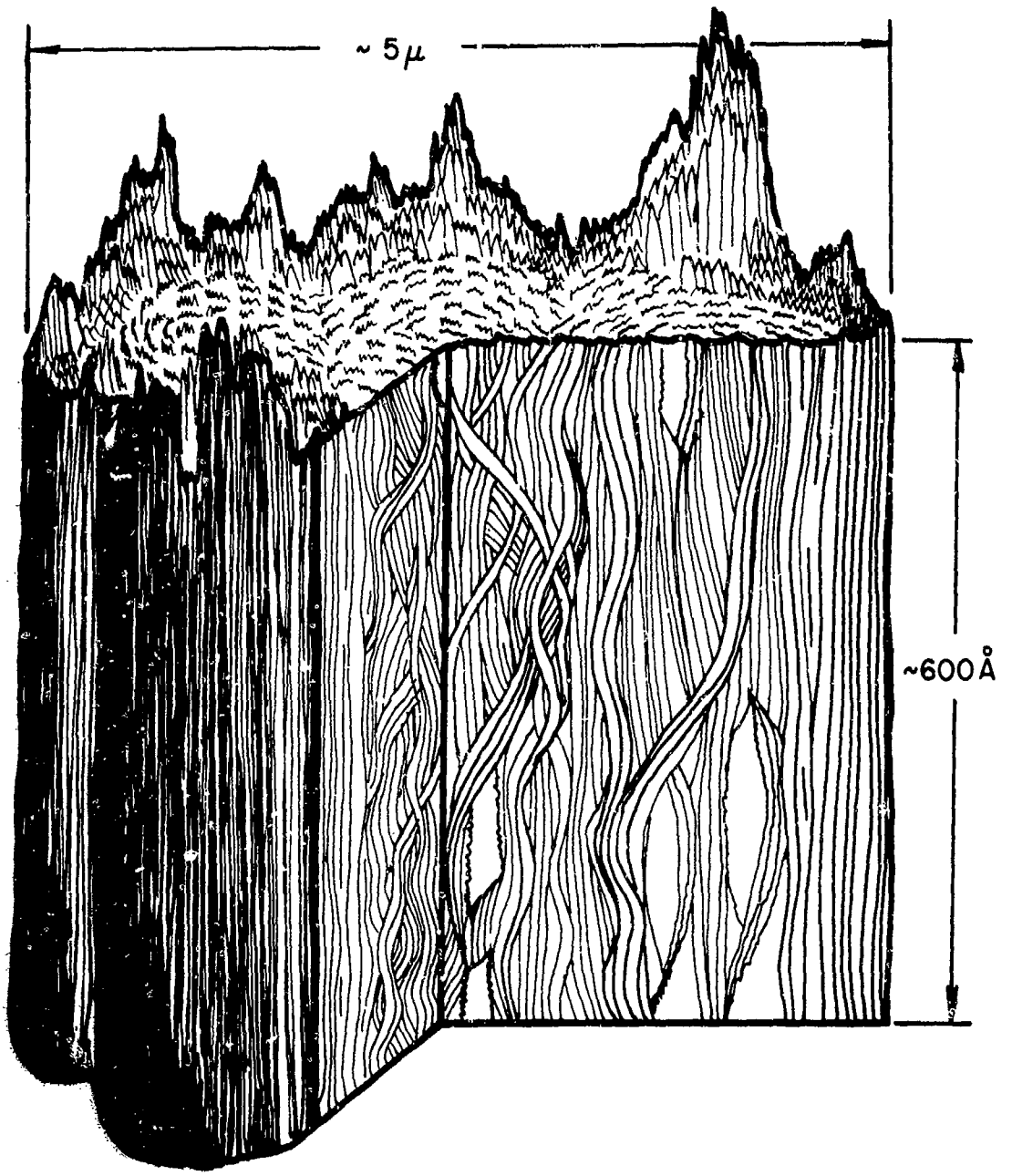

Fig. 31 Schematic 3-D structural model of CS-4.

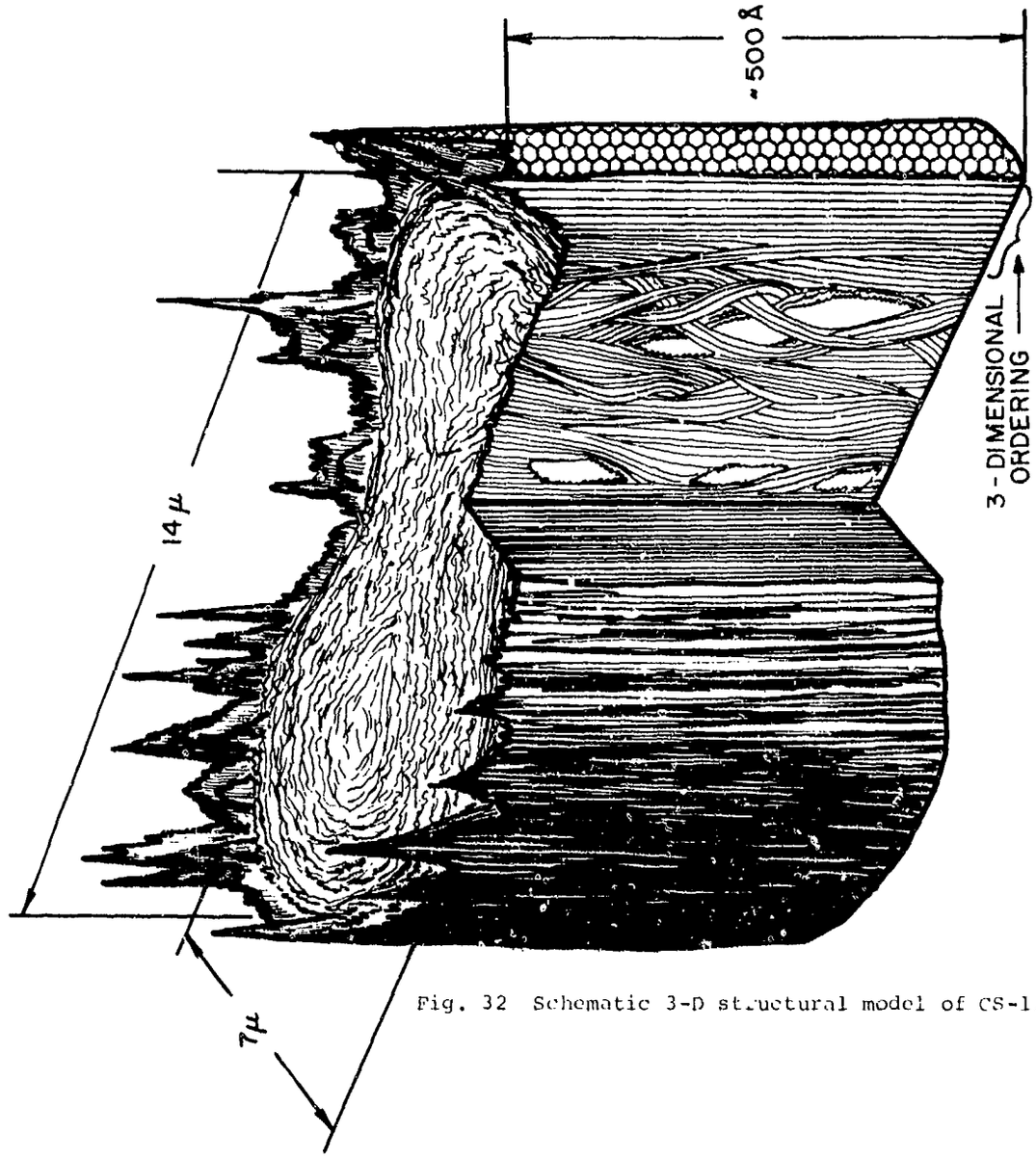

Fig. 32 Schematic 3-D structural model of CS-1.

6. CS-3, E = 104 x 10^6 psi.

A schematic of the structure of CS-3 is shown in Fig. 33. The irregular cross-sectional shape is indicative of a rayon base. Significantly, CS-3 departs from some of the preceding trends by having a d_{002} of 3.41Å and a relatively small l_c of 64Å; $W_{\frac{1}{2}}$ is 11° however. Replicas reveal the surface to be like CS-1, locally ver smooth and rippled indicative of a highly graphitic nature. (0002) dark fields show a highly preferred structure, but no cross-correlation of diffracting areas is present as in CS-1. Radially, two types of fibers exist; those of complex optical interaction, and those of larger dimensions, that probably broke during stretching, with little or no development. SEM photographs suggest a centro-symmetric basal wrap around structure, however.

7. CS-5, E = 116 x 10^6 psi.

CS-5, Fig. 34, has a dog-bone cross-section. The low $W_{\frac{1}{2}}$ of 10° is consistent with the very high modulus; in addition, CS-5 has a large l_c of 203Å and a low d_{002} of 3.37Å, once again probably due in part to the catalysis. The surface is smooth, and (0002) dark field photographs confirm the existence of a well developed surface structure. Overall too the fiber is well developed, and consequently the fracture profile is very rough. The microfibrils are almost linear. Optically, a poorer structure is present in the cores of the fiber lobes, and from reverse sputtering results it may be inferred that CS-5 is composed of at least three areas; a

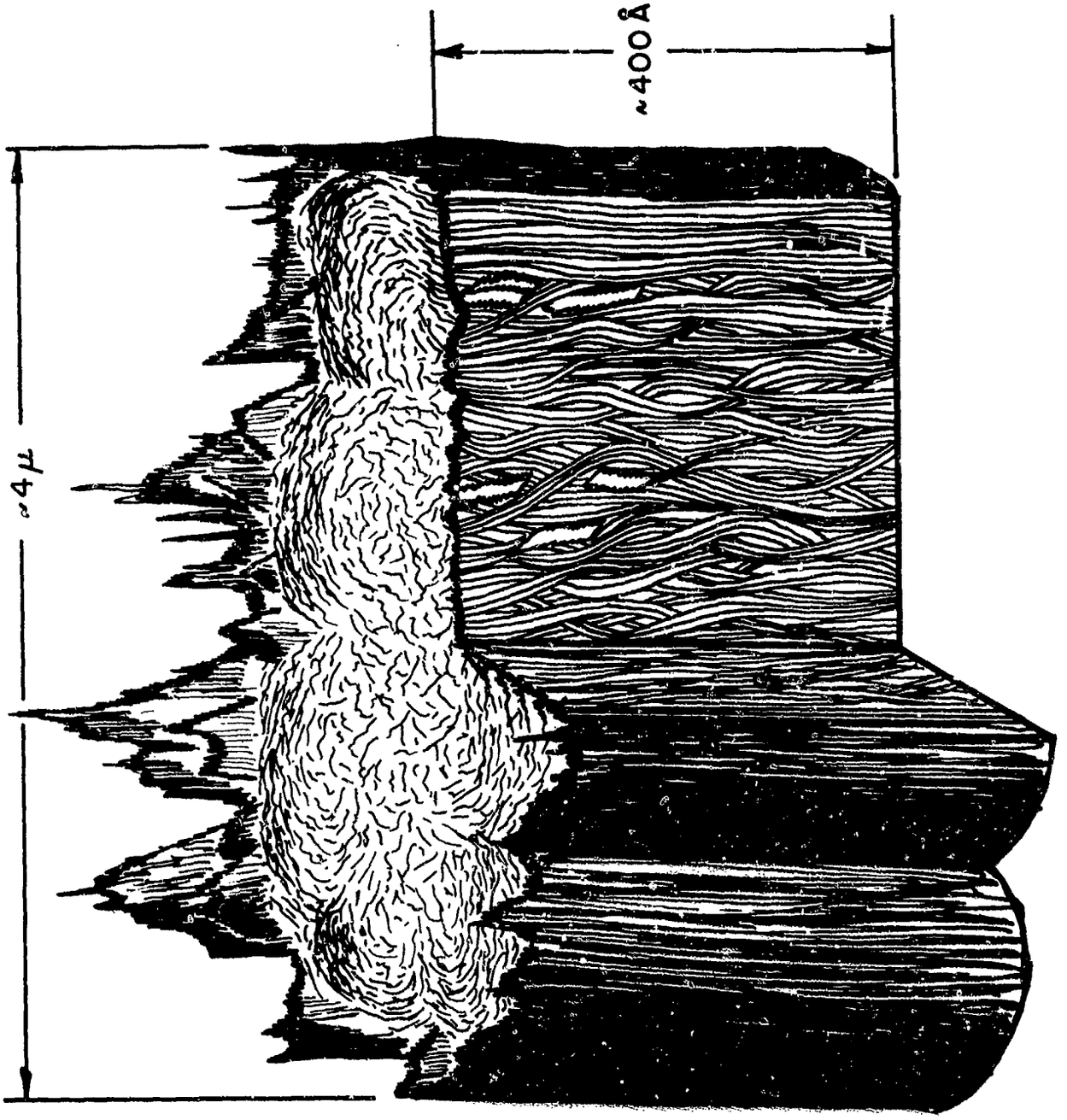

Fig. 33 Schematic 3-D structural model of CS-3.

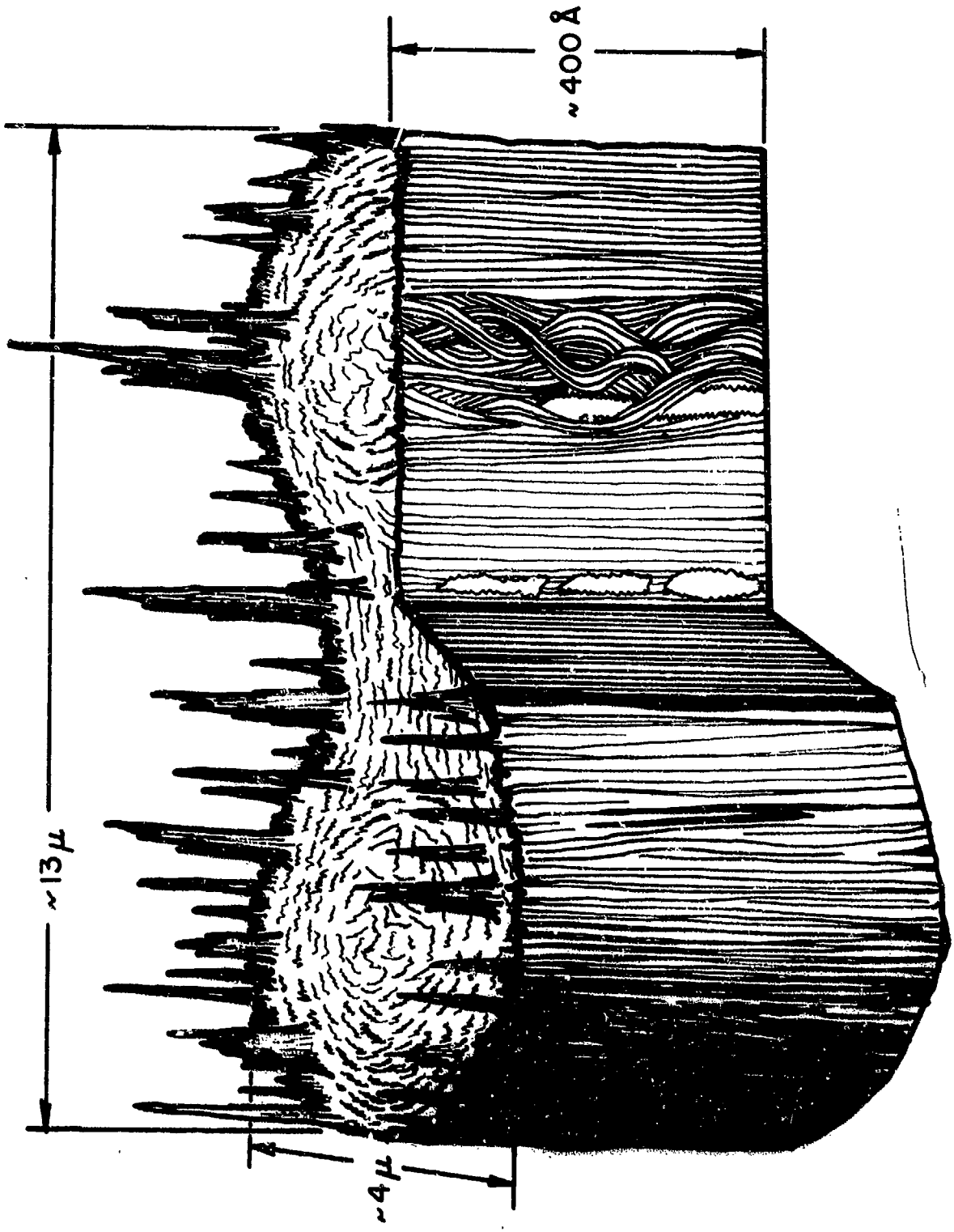

Fig. 34 Schematic 3-D structural model of CS-5.

well aligned outer shell of onion skin morphology, the random lobe cores, and a narrow intermediate region. This multi-structure may explain the apparently low preferred orientation as seen from Debye-Scherrer, and the higher than expected d_{002}; i.e., there may be significant amounts of residual stress present.

SECTION V

CONCLUSIONS

Carbon fibers consist of long undulating and twisting ribbons. For fibers with a modulus of 6 million psi., there is almost a random orientation of these ribbons with respect to the fiber axis. The thickness of these ribbons is approximately 5 to 6 turbostratic layer planes with a width of probably 20Å. The ribbons are highly undulated and twisted to give an inter-tangled mass. This provides a tight coupling between ribbons, and the fibers are observed to be surface flaw sensitive. Only a small portion of the surface appears to be covered with basal plane, and interfacial bonding to the matrix should be good. Flaw sensitivity should give a high gauge length effect with tensile strength, with short gauge lengths giving much higher strengths. Combined with good bonding, this should give a high "translation" of fiber strength (measured at 1 inch gauge length) to the composite.

For fibers with a 41 million modulus, the ribbons are typically about 13 layer planes thick and 40Å wide. The amplitude of the undulation is greater than the wavelength, and about three-quarters

of the basal planes are aligned within 30° of the fiber axis. Some variation in preferred orientation from the surface of the fiber to the center is observed, with the surface having a higher preferred orientation. There is also some radial preferred orientation with basal planes orienting parallel to the fiber surface. The interior radial preferred orientation depends on the processing, but is lower than the surface. The variation in axial preferred orientation and the radial preferred orientation will give rise to residual stresses upon cool-down. These stresses are compressive axially and circumferentially at the surface, and tensile radially. The combination of radial residual stress with a lowered tangling of the ribbons gives poorer coupling between ribbons. Fractography also shows rougher fracture surfaces. The uncoupling of the ribbons and the compressive surface stresses also appear to make the fiber somewhat less flaw sensitive. However, tensile strength gauge length effects are still relatively large. The fiber surface is starting to be covered with appreciable amounts of basal plane, but the resin bonding to the surface is still relatively high. The variation in axial preferred orientation will also cause the outside sheath of the fiber to carry more of the load. The interaction of this non-uniform loading with the residual stress has not been determined. The good bonding and high tensile strength at short gauge lengths should give good "translation" of the length fiber strength to the composite.

For 50 million psi fiber, the ribbons remain turbostratic and increase to about 20 layers thick and 70Å wide. The undulation amplitude drops to less than the wavelength, and three quarters of basal planes are oriented within 12° of the fiber axis. Less tangling is observed between ribbons, and a high radial preferred orientation is observed with the basal planes parallel to the surface. The residual stress which develops from the radial preferred orientation becomes high enough to cause internal fracture, which, with less tangling of the ribbons, gives poor coupling between ribbons. Fiber fracture surfaces become quite rough, and the tensile strength of the fiber often decreases. Flaw sensitivity and tensile strength gauge length affects decrease. The surface of the fiber is predominantly a faulted basal plane, and interfacial bond strength, without etching, will be low. Translation of fiber tensile strength, for surface treated specimens, to composite properties will be reduced as the strength at short gauge length does not increase as rapidly as for flaw sensitive fibers of lower modulus.

Finally, for fibers of 100 million modulus, the ribbons are about 30 layers thick and 90Å wide, but ribbon fusion is evident in some samples. For one PAN sample, three dimensional ordering was observed, together with a preferred orientation of a-axes. The orientation was that expected if the orientation of carbon backbone of the PAN polymer was retained throughout processing. The

ribbons are observed to have almost zero amplitude and are essentially parallel to the fiber axis. Very little tangling is also observed. Strong radial preferred orientation occurs, and the resulting residual stresses must give very poor coupling between ribbons. Fracture surfaces are extremely jagged. The fiber surface consists of extremely smooth basal planes which would give poor bonding.

The strong similarities among carbon fibers of the same modulus, but from different precursors, were more noteworthy than the differences. Axial structures appeared very similar with catalytically processed fibers having somewhat larger l_c values; differences were more apparent in radial structures. In general, however, higher radial preferred orientations were associated with higher axial preferred orientations. Samples which appear to be strain-annealed show a somewhat poorer development of radial structure as might be expected.

Finally, improved carbon fibers are conceivably possible if axial alignment of ribbons can be accomplished with a minimum of radial alignment. This would minimize decoupling of ribbons.

FUTURE WORK

In the next year efforts will be made to obtain electron diffraction measurements of fibers using reverse sputtering to progressively etch away controlled amounts of fiber surface in order to measure any d_{002} gradients from fiber surface to core.

Further optical development will be pursued so that more quantitative radial characterization will be possible. In addition, radial and x-ray determined preferred orientations will be carefully compared and evaluated.

Small angle scattering will be used to investigate porosity distributions.

APPENDIX I

X-RAY CORRECTION PROCEDURE FOR d_{002} AND l_c

Linear subtraction of a straight baseline drawn between the two minima on either side of the (0002) peak approximately corrects for independent scattering, Compton Modified Scattering, M_1 or single layer scattering, and small angle scattering. Division of the resultant curve was then done to correct for the atomic scattering factor and Lorentz Polarization. It was assumed that the absorption and temperature factors cancelled. Machine broadening was determined from a very well annealed pyrolytic graphite sample (16 hours at 3600°C) and subtracted at one-half the maximum intensity using variance subtraction. The results are not adjusted for possible residual strain components. Basal atomic spacing, d_{002}, was subsequently calculated using the value of 2θ at the resulting maximum intensity. Crystallite sizes in the c direction were calculated by the Scherrer formula:

$$L_c = \frac{0.89\lambda}{B \cos \theta_B}$$

where B was measured at one-half the maximum intensity.

APPENDIX II

REFLECTED POLARIZED LIGHT THEORY

Graphite is optically classified as a uniaxial absorbing material possessing two distinct refractive indices and absorption coefficients characteristic of basal and c-axis directions. In the most general case light, which is plane polarized and vertically incident on such a material, is reflected as elliptically polarized light. It is the analysis of the elliptical character and the subsequent correlation with known crystallographic orientations that makes the determination of any radial preferred distribution in carbon fibers possible. The analysis is as follows:

Consider first the case of a single crystal resting on the stage of an optical microscope with the light incident on a normal face as in Fig. 35. This incident light is plane polarized and has its azimuth of vibration parallel to PP. Originally the analyzer (AA) is crossed with the polarizer. The dashed lines represent the traces of basal edge perpendicular to the microscope stage and oriented at 45° to the nicols. In this orientation the interaction may be vectorially described as in Fig. 36.

$\overline{OE}$ represents the magnitude and direction of the incident light. With the material in the 45° position as above, the light is resolved into two equal components $\overline{OE}_1$ and $\overline{OE}_2$; $\overline{OE}_1$ is parallel to the basal plane, $\overline{OE}_2$ is parallel to the c-axis. These components, then interact with the material and are reflected in different

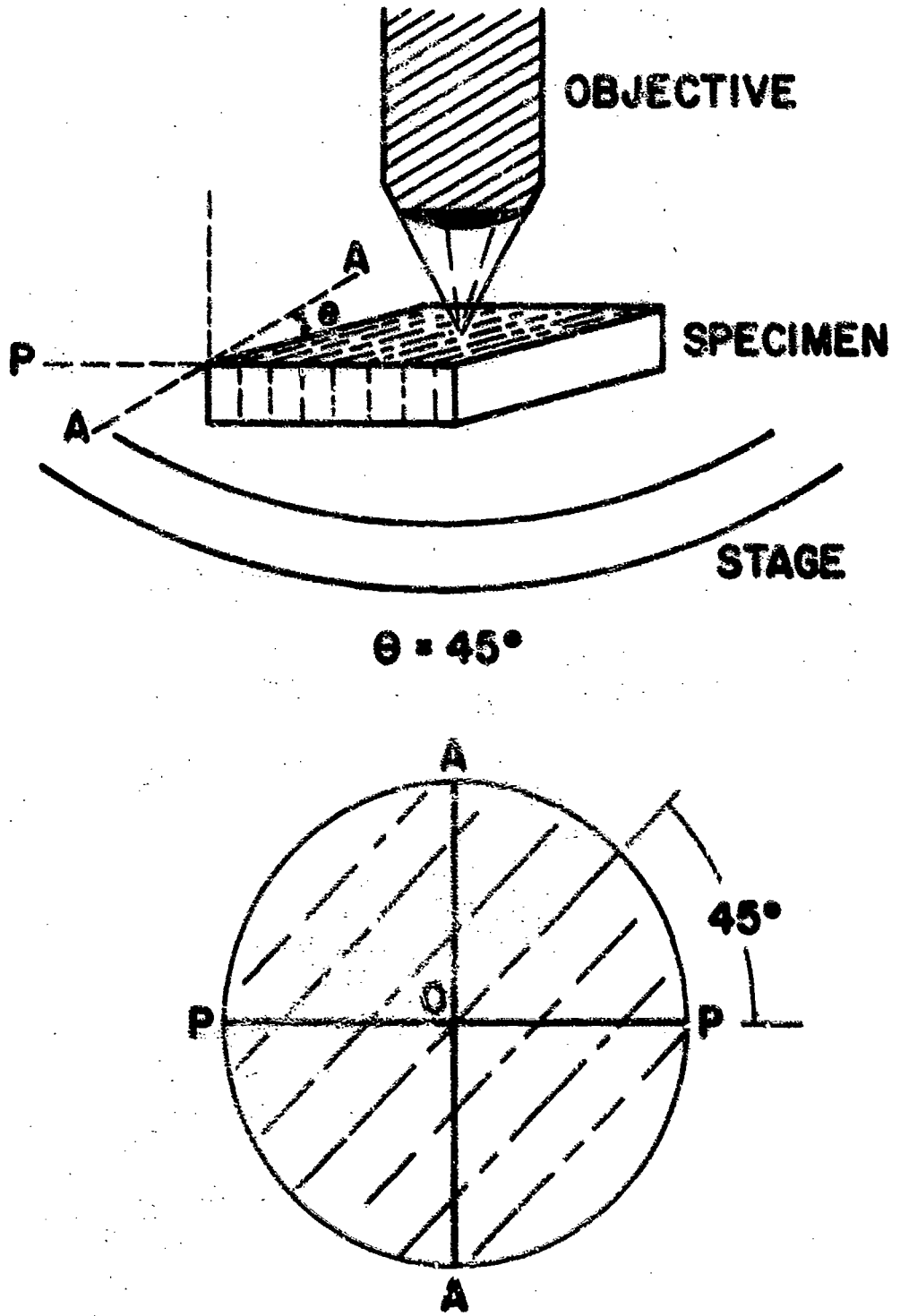

Fig. 35 Schematic of anisotropic single crystal resting on microscope stage.

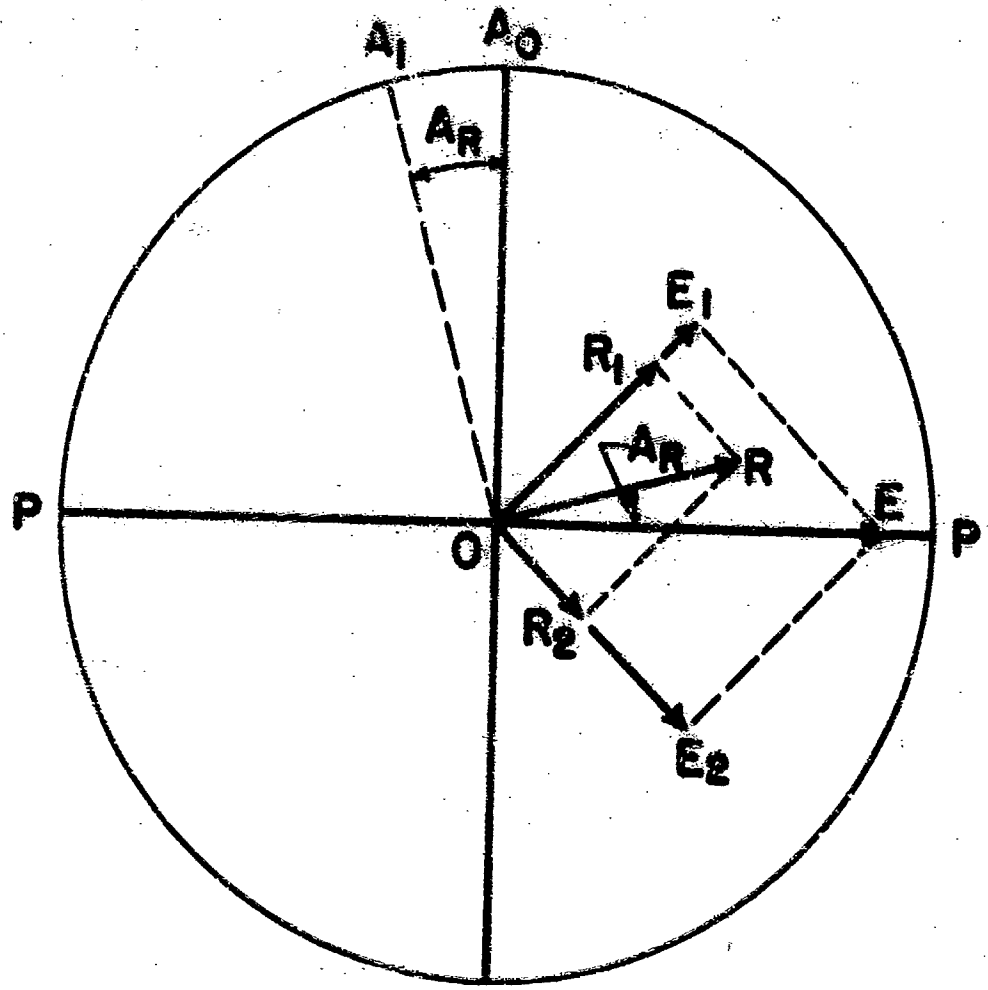

Fig. 36 Vectorial light analysis diagram.

amounts according to:

$$R_w = \frac{(n_w - 1)^2 + k_w^2}{(n_w + 1)^2 + k_w^2}$$

$$R_\epsilon = \frac{(n_\epsilon - 1)^2 + k_\epsilon^2}{(n_\epsilon + 1)^2 + k_\epsilon^2}$$

where: $R_w = \frac{\overline{OR}_1}{\overline{OE}_1}$

$$R_\epsilon = \frac{\overline{OR}_2}{\overline{OE}_2}$$

n_w - index of refraction in the basal plane

n_ϵ - index of refraction parallel to the c-axis.

k_w - absorption coefficient in basal plane

k_ϵ - absorption coefficient parallel to the c-axis.

R_w and R_ϵ are termed the uniradial reflectivities of the basal and c-axis directions respectively. The resultant is $\overline{OR}$ whose magnitude is less than the incident vector $\overline{OE}$, and whose plane of polarization has been rotated counterclockwise by angle A_R. If $\overline{OR}_1$ and $\overline{OR}_2$ are vibrating in phase, a rotation of the analyzer to A_1 by angle A_R will completely extinguish the image. In the general situation however, $\overline{OR}_1$ and $\overline{OR}_2$ are not in phase (circular or elliptical polarization), and a method of compensating for this must be introduced. This purpose is served by inserting a variable compensation plate below the analyzer and rotating the plate to get total extinction. The plate, when positioned at compensation,

retards one of the reflected components more than the other to the point where $\overline{OR}_1$ and $\overline{OR}_2$ are in phase. In most cases the azimuth of A_R is changed to a different value $A_{R\beta}$. A true extinction angle may then be calculated according to:

$$\cos 2 A_R = \cos A_{R\beta}/\cos 2\nu$$

where ν is the measured phase angle. The above analysis is after Berek[4]; unfortunately, the method has several disadvantages. The final setting of the analyzer is dependent on the compensator setting, which involves significant precision problems. This results in large errors in calculated A_R values. Secondly, the measured specific total compensation of mica plates varies so that it is difficult to compare results among different observers.

A second method recommended by Cameron[5], after Hallimond, increases precision. The experimental technique involves the use of a Nakamura plate to increase the ability to detect the position of minimum light intensity without compensation. The results are more reproducible even though the phase difference component is not taken into account. The measured angle is termed the apparent rotation angle, $A_R°$.

Measurements of the apparent rotation angle were made on bulk samples of well annealed pyrolytic graphite using white light after R.F. sputter polishing. No Nakamura plate was available, but significant differences were found none-the-less. The value of A_R in the basal plane was found to be 0°.

Next, a sample was oriented with the basal planes normal to the microscope stage as in Fig. 37. The angle between the original analyzer direction, A_O, and the basal cleavage is θ. The sample was rotated in 10° increments and A_R measured at each position. Other specimens were prepared such that the angles between the basal planes and incident beam (ϕ) were different as in Fig. 38; the variation in A_R was then determined with ϕ as above. The results are plotted in Fig. 39. The values of A_R as a function of ϕ at the 45° position are plotted in Fig. 40.

From this plot it may be inferred that if the angle between the basal planes and the fiber axis is about 30° or more, the fiber cross-section should be essentially extinct in polarized light (crossed polars) regardless of the radial (θ) distribution. If ϕ is significantly less than 30°, radial variations in A_R may be observed.

The implications of this point are important. Consider the case of a fiber with a "tree trunk" cross-sectional structure whose basal planes are very nearly aligned parallel to the fiber axis as shown in Fig. 41a. The dashed lines represent basal traces. Since $\phi \approx 0°$, only the top curve in Fig. 39 need be used. For purposes of discussion, divide the circular cross-section into eight sectors as indicated in Fig. 41b. Once again the dashed lines represent basal traces, only this time it is assumed that the radial distribution may be approximated as octagonally centrosymmetric. Thus for $\phi \approx 0°$:

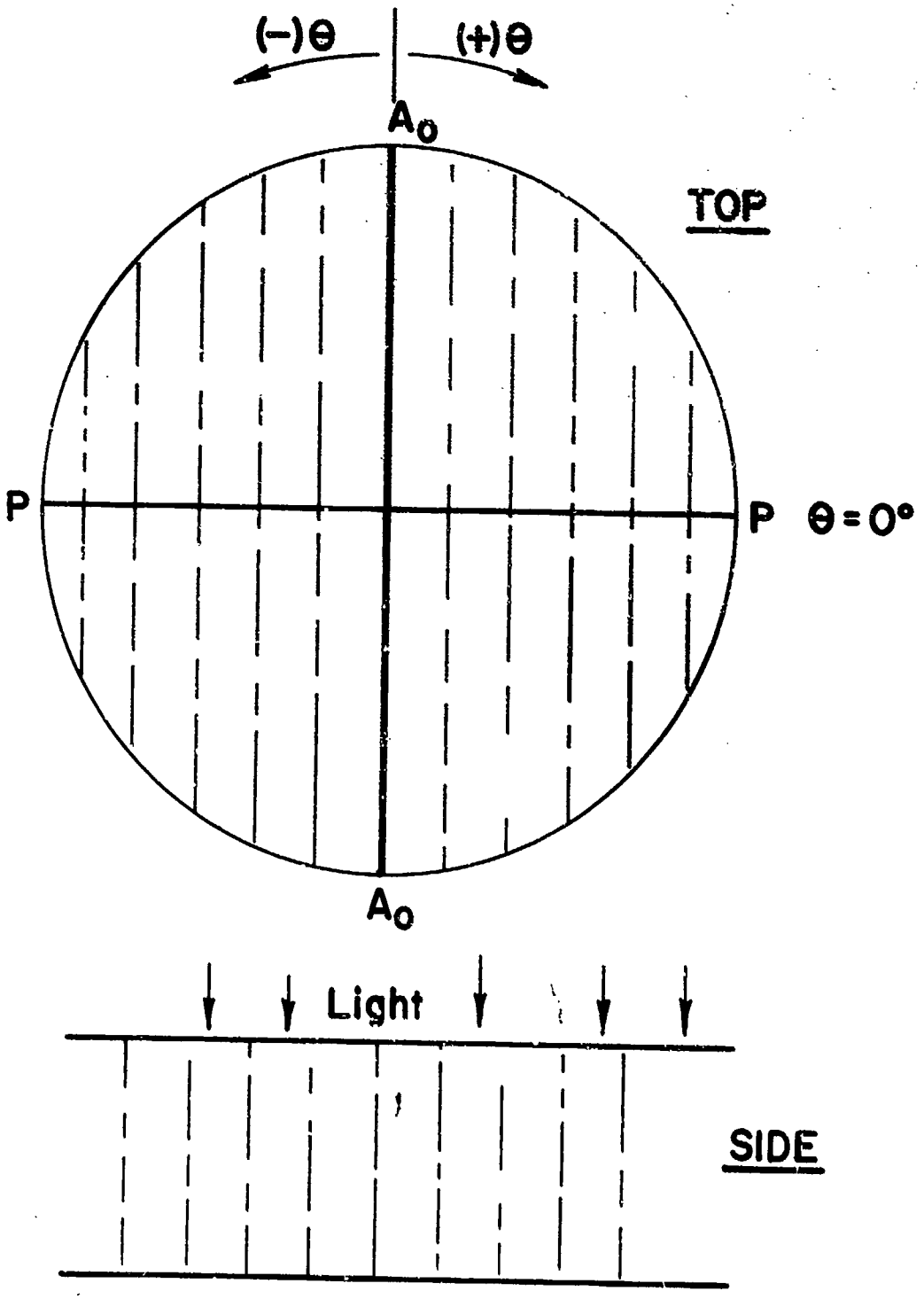

Fig. 37 Schematic of initial measurement position $\phi = 0°$.

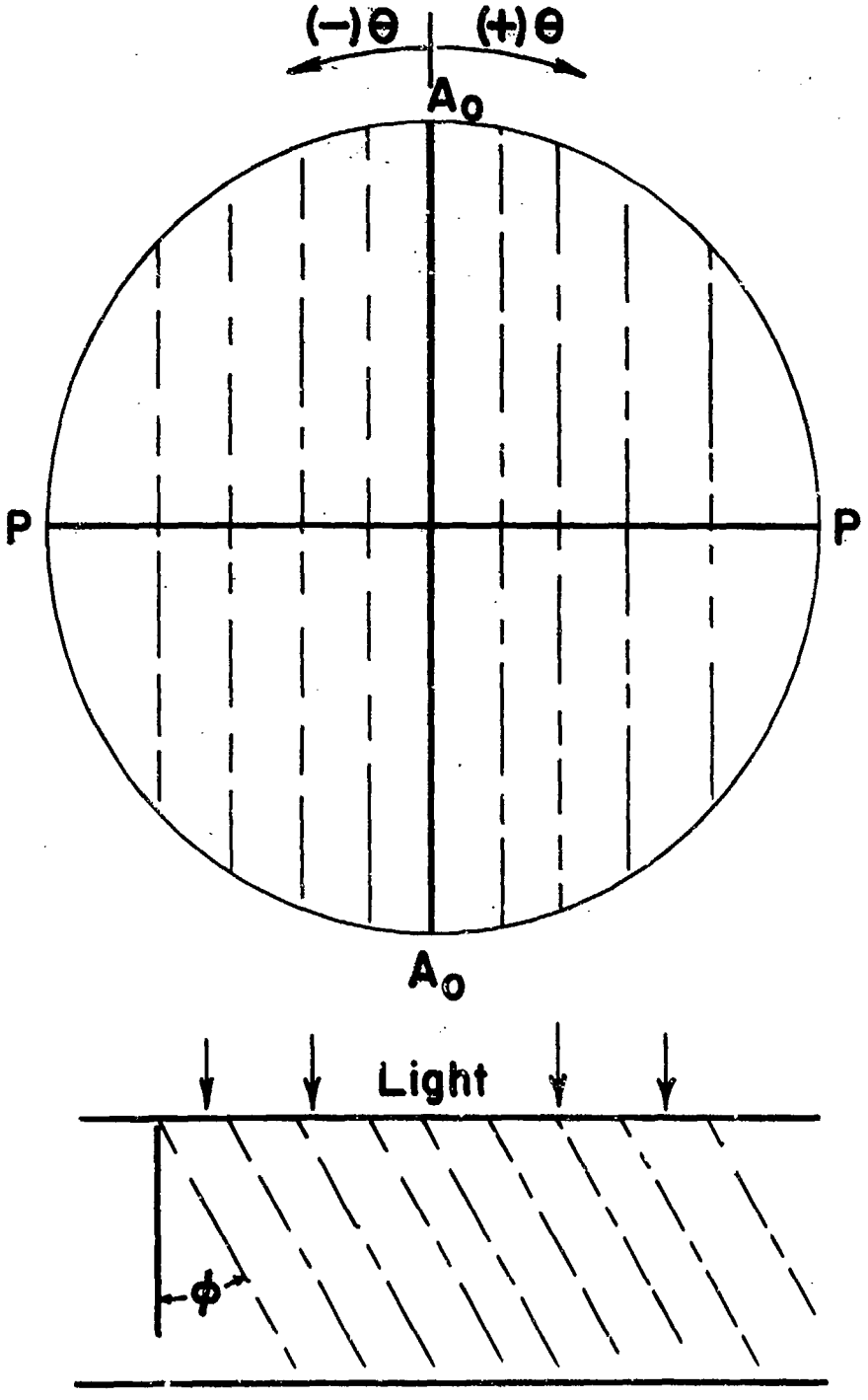

Fig. 38 Schematic of initial measurement position $\phi \neq 0°$.

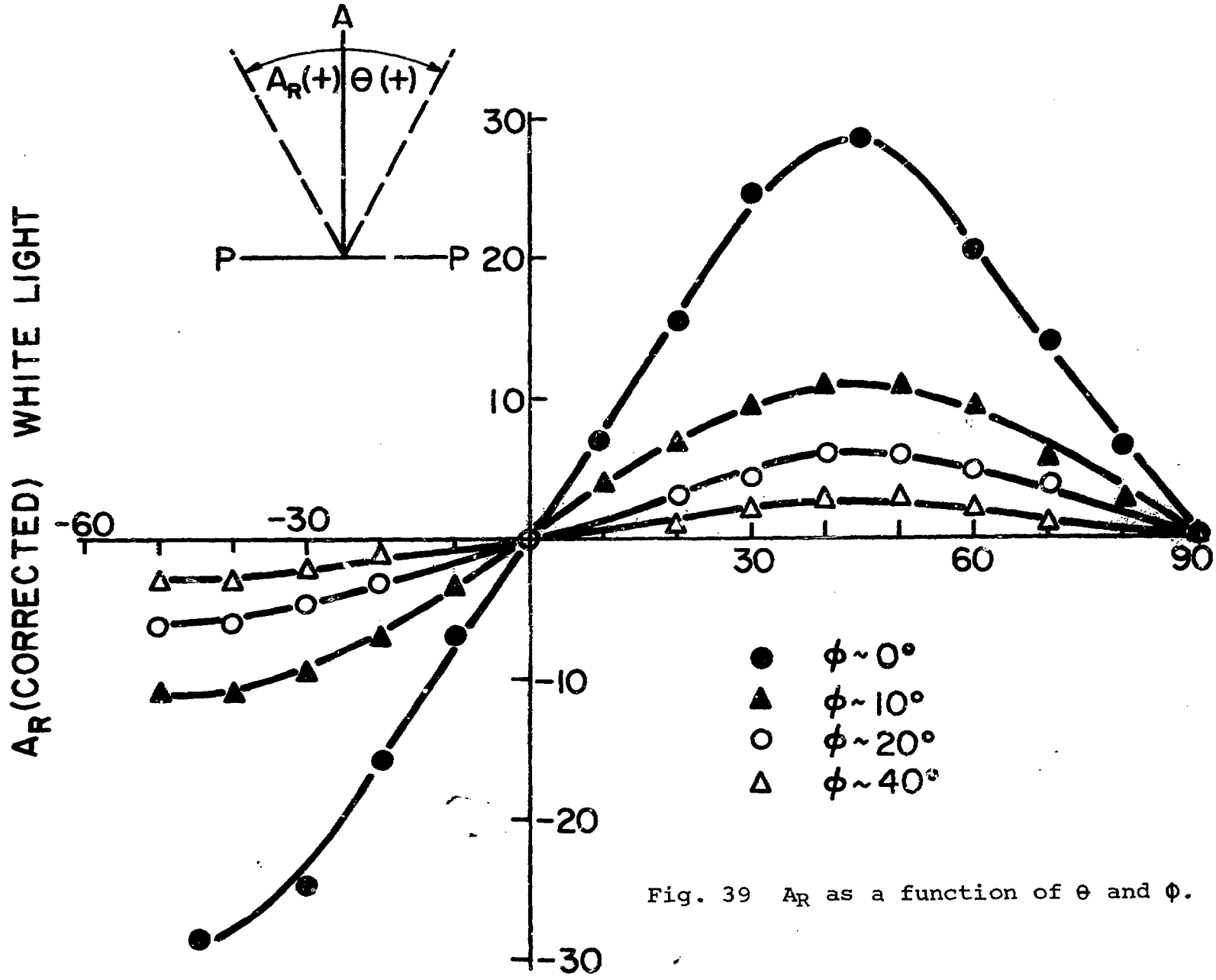

Fig. 39 A_R as a function of θ and φ.

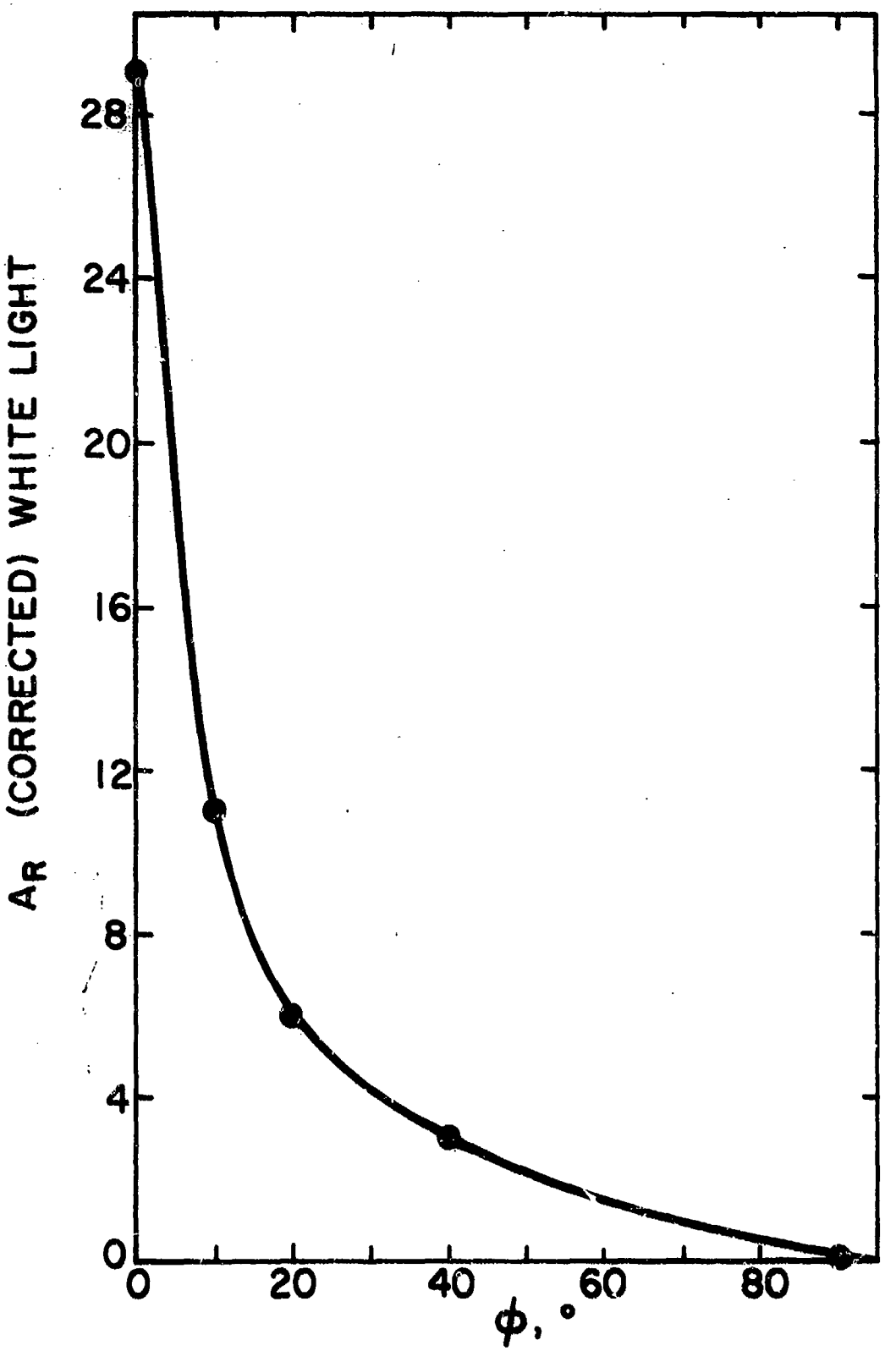

Fig. 40 A_R as a function of ϕ at $\theta = 45°$

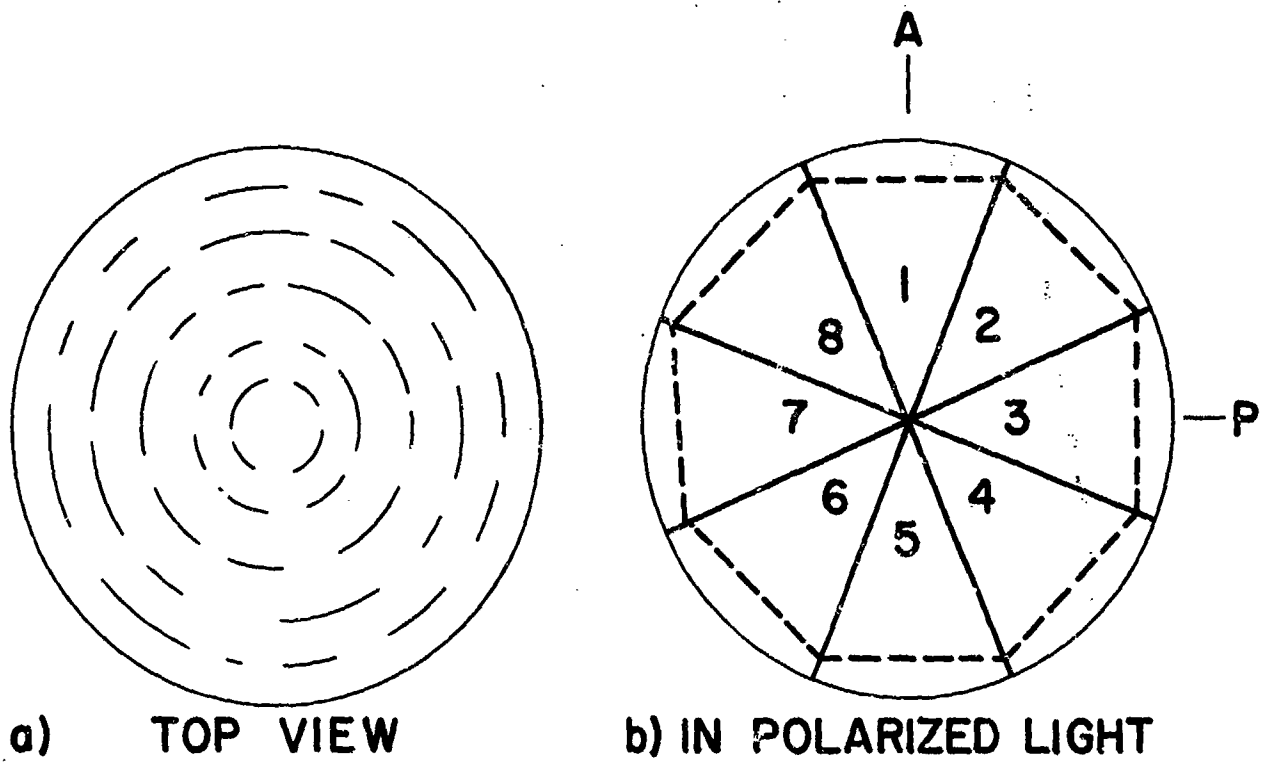

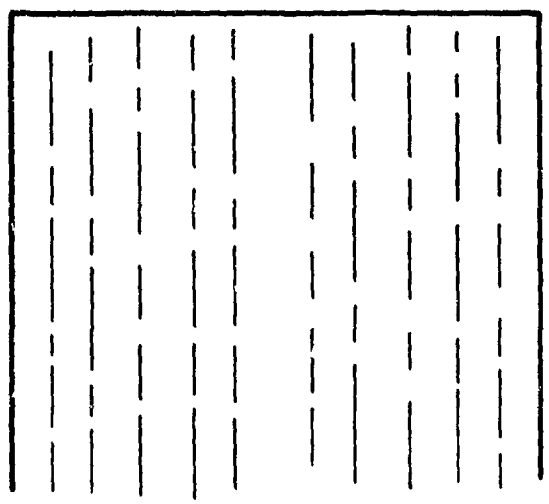

SIDE VIEW (CUT)

Fig. 41 Schematic of ideal onion skin fiber.

Sector	θ
1	90
2	-45
3	0
4	45
5	90
6	-45
7	0
8	45

In crossed polars sectors 1, 3, 5 and 7 would be extinct giving rise to a "Formee Cross of Heraldry" pattern. Rotation of the analyzer by about 25° counterclockwise would cause sectors 4 and 8 to become extinct, the rest of the fiber now light.

A second case to be considered is a radial basal distribution as in Fig. 42. Again, assuming $\phi \approx 0°$, sectors, 1, 3, 5 and 7 would be dark between crossed polars. This time however, rotation of the analyzer counterclockwise by 25° would break-up the polarization figure and sectors 2 and 6 would be extinct, the rest of the fiber lighter.

A final basic case would be a random radial distribution of basal planes still having $\phi \approx 0°$ as in Fig. 43. Since, at all orientations of the analyzer to 28.5°, there will be a constant proportion of all c-axis orientations, the cross-section will be uniformly but partially extinct. The whole section will become light after the 28.5° point is exceeded.

Consider a more complicated case, that of a dog-bone shaped fiber whose central end lobe sections are random, but the skin of the fiber is of highly basal character as in Fig. 44a. The fiber

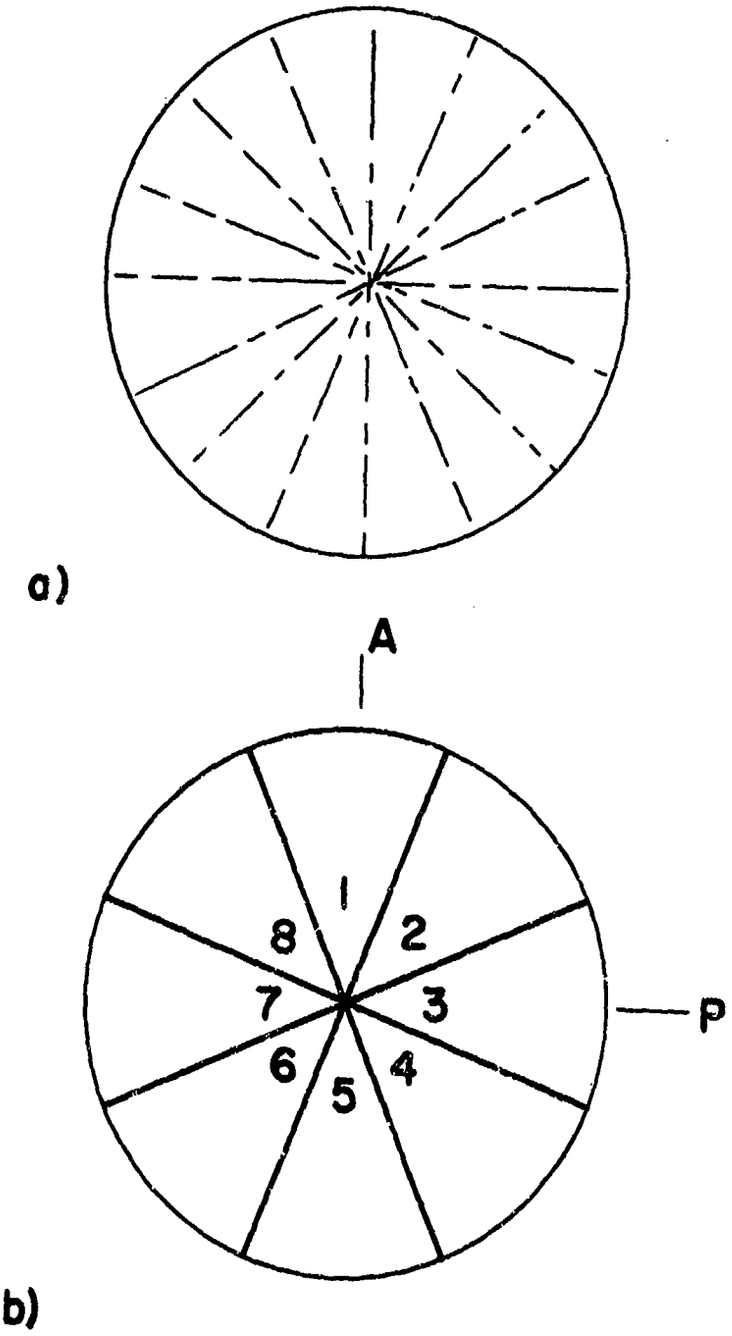

Fig. 42 Schematic of ideal spoke radial configuration.

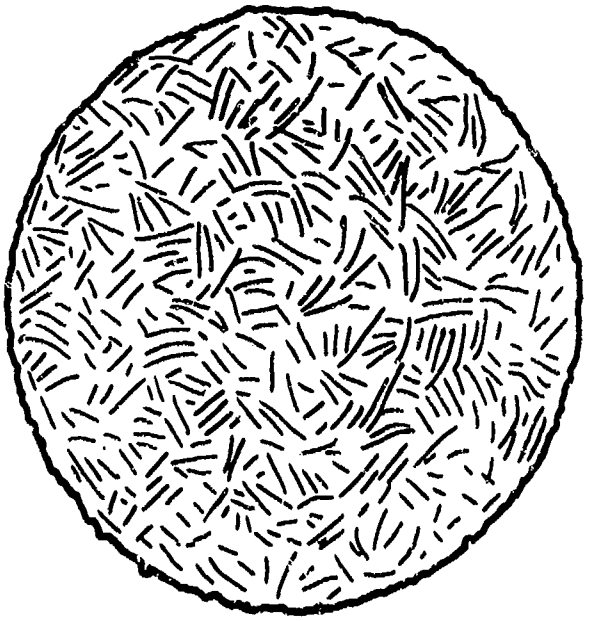

Fig. 43 Schematic of fiber having a random radial distribution.

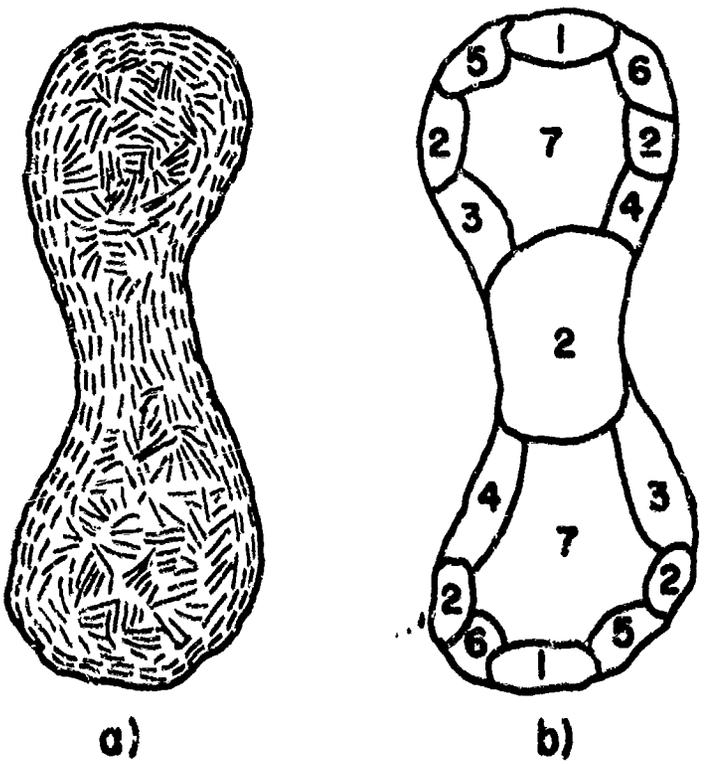

Fig. 44 Schematic of a dogbone shaped fiber with an assumed radial distribution.

is schematically divided into seven regions of equivalent optical orientation as in Fig. 44b. Assuming $0 \approx 0°$ again, the fiber should behave optically as in Fig. 45 for the particular values of the analyzer settings. This general behavioral scheme has been observed for a larger than average CS-1 fibers. The size difference suggested the fiber may have broken before or during the stretching procedure thus giving rise to the random core lobe sections.

Fig. 45 Optical behavior of fiber given in Fig. 44 as analyzer is rotated.

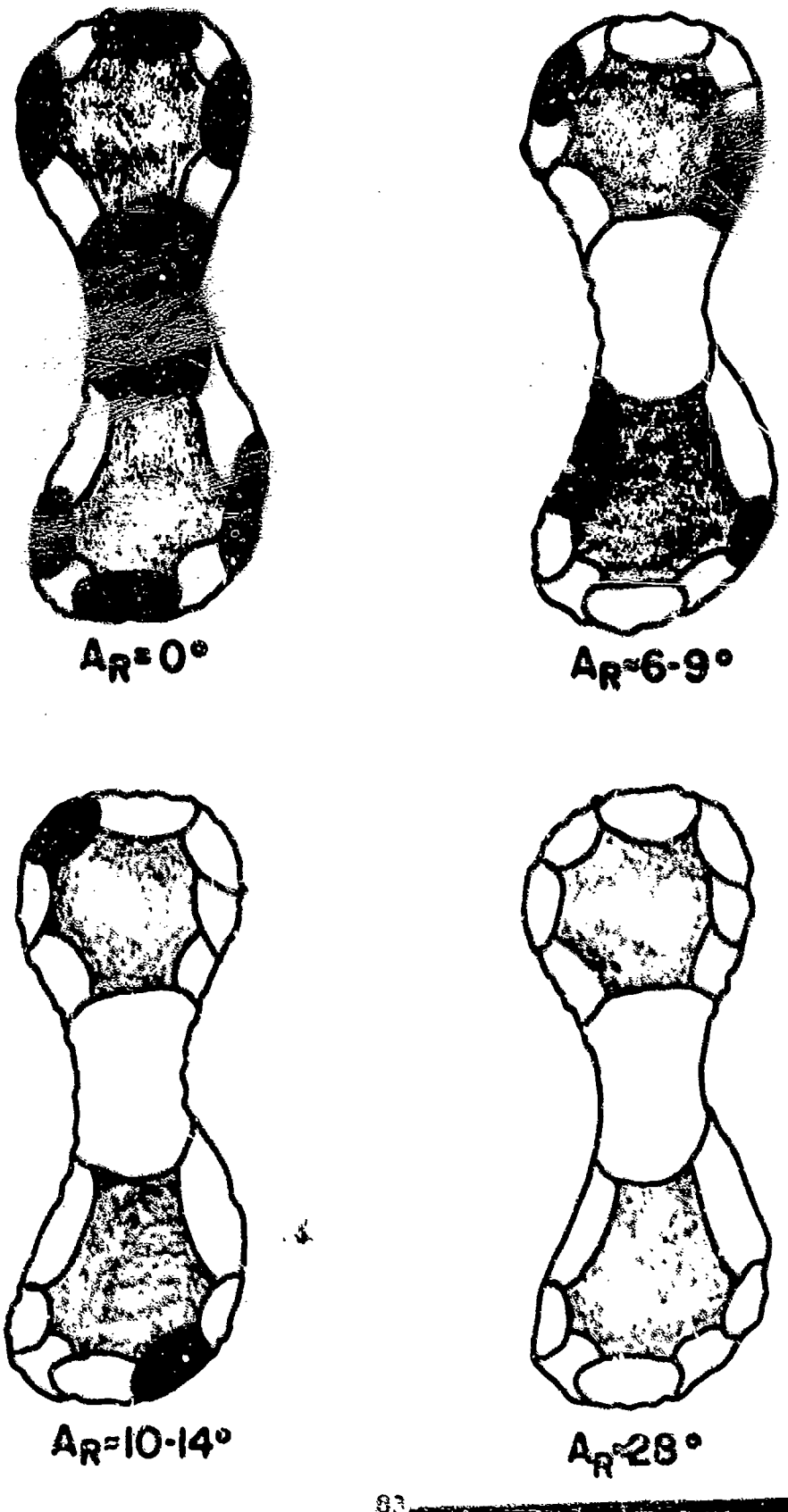

END